TURUN
YLIOPISTO
UNIVERSITY
OF TURKU

# MULTIMODALITY IMAGING IN PROSTATE CANCER

Anna Kuisma

TURUN YLIOPISTON JULKAISUJA – ANNALES UNIVERSITATIS TURKUENSIS
SARJA – SER. D OSA – TOM. 1685 | MEDICA – ODONTOLOGICA | TURKU 2023

TURUN
YLIOPISTO
UNIVERSITY
OF TURKU

# MULTIMODALITY IMAGING IN PROSTATE CANCER

Anna Kuisma

TURUN YLIOPISTON JULKAISUJA – ANNALES UNIVERSITATIS TURKUENSIS
SARJA – SER. D OSA – TOM. 1688 | MEDICA – ODONTOLOGICA | TURKU 2023

## University of Turku

Faculty of Medicine
Clinical Oncology
Doctoral programme in Clinical Research
Department of Oncology and Radiotherapy
Clinical Physiology, Nuclear Medicine and Turku PET Centre

## Supervised by

Professor Heikki Minn
Department of Oncology and Radiotherapy
Turku University Hospital
University of Turku
Turku, Finland

Adj. Professor Marko Seppänen
Department of Clinical Physiology, Nuclear Medicine and PET Centre
Turku University Hospital
University of Turku
Turku, Finland

## Reviewed by

Adjunct Professor, Antti Loimaala
Chief Physician
Helsinki University Hospital
Department of Nuclear Medicine
Meilahti Hospital Diagnostic Center
Helsinki, Finland

Adjunct Professor, Juha Nikkinen
Oulu University Hospital
Department of Radiotherapy
Oulu, Finland

## Opponent

Docent Leila Vaalavirta, M.D., Ph.D.
Chief Physician
Wellbeing services county of Kymenlaakso
Kotka, Finland

The originality of this publication has been checked in accordance with the University of Turku quality assurance system using the Turnitin OriginalityCheck service.

ISBN 978-951-29-9137-2 (PRINT)
ISBN 978-951-29-9138-9 (PDF)
ISSN 0355-9483 (Print)
ISSN 2343-3213 (Online)
Painosalama, Turku, Finland 2023

UNIVERSITY OF TURKU
Faculty of Medicine
Clinical Oncology
Department of Oncology and Radiotherapy and Clinical Physiology, Nuclear Medicine and Turku PET Centre, University of Turku, Turku University Hospital, Turku Finland
ANNA KUISMA: Multimodality Imaging in Prostate Cancer
Doctoral Dissertation, 113 pp.
Doctoral Program in Clinical Research
January 2023

## ABSTRACT

Prostate cancer is the most common cancer in men in Finland. Its aggressiveness varies widely, from indolent to fatal disease. Accurate characterization of prostate cancer is extremely essential to prevent overtreatment while sustaining good survivorship and high quality of life. This is feasible using novel technology in imaging and automatic tools in treatment planning.

In the first part of this thesis work, the aim was to evaluate anti-1-amino-3-$^{18}$F-fluorocyclobutane-1-carboxylic acid ($^{18}$F-FACBC) PET/CT, PET/MRI, and multiparametric MRI (mpMRI) in detection of primary prostate cancer. The uptake of $^{18}$F-FACBC was significantly stronger in tumors with higher Gleason score and it may therefore assist in targeted biopsies when combined with MRI. $^{18}$F-FACBC PET/MRI outperformed PET/CT but did not demonstrate higher diagnostic performance than mpMRI performed separately. Furthermore, PET/MRI and mpMRI failed to detect pelvic lymph node metastasis measuring less than 8mm. $^{18}$F-FACBC PET/MRI is promising in characterization of primary prostate cancer, especially if ablative treatments are planned. It is not likely to replace mpMRI in clinical practice.

The second study assessed multimodality imaging in detecting bone metastasis in high-risk prostate cancer and breast cancer patients. All patients underwent $^{99m}$Tc-HDP bone scintigraphy (BS), $^{99m}$Tc-HDP SPECT, $^{99m}$Tc-HDP SPECT/CT, $^{18}$F-NaF PET/CT, and whole body (wb) MRI+DWI. $^{99m}$Tc-HDP SPECT/CT, $^{18}$F-NaF PET/CT, and wbMRI+DWI had superior sensitivity compared to conventional nuclear imaging. In particular non-BS techniques showed less equivocal findings. wbMRI+DWI was as accurate as $^{18}$F-NaF PET/CT for detecting bone metastasis and may be considered a potential "single-step" imaging modality for detection of bone metastasis in high-risk patients with prostate and breast cancer.

The purpose of the third study was to evaluate and validate the performance of a fully automated segmentation tool (AST) in MRI-based radiotherapy planning of prostate cancer. It showed high agreement for delineating prostate, bladder, and rectum, compared to manual contouring, and suggested adoption of AST in clinical practice.

Finally, the fourth study investigated the long-term toxicity after biologically guided radiotherapy in men with localized prostate cancer. Carbon-11 acetate ($^{11}$C-ACE) PET-CT was used to guide dose escalation into metabolically active intraprostatic lesions. $^{11}$C-ACE PET-guided radiotherapy was feasible and well tolerated. Although erectile dysfunction was relatively common, severe gastro-intestinal symptoms were very rare, and no grade 3 genitourinary symptoms were present at five years after radiotherapy.

The findings of this thesis have potential to improve diagnostic imaging and radiotherapy planning in primary and metastatic prostate cancer. Eventually, they are likely to improve patients' quality of life and survival.

KEYWORDS: prostate cancer, magnetic resonance imaging, positron emission tomography, radiotherapy planning, toxicity, bone metastasis

TURUN YLIOPISTO
Lääketieteellinen tiedekunta
Kliininen Syöpätautioppi
Syöpätautien klinikka
PET-keskus
Turun Yliopistollinen keskussairaala
ANNA KUISMA: Biologisen kuvantamisen käyttö eturauhassyövässä
Väitöskirja, 113 s.
Turun Kliininen Tohtoriohjelma
Tammikuu 2023

## TIIVISTELMÄ

Eturauhassyöpä on miesten yleisin syöpä Suomessa. Sen taudinkuva vaihtelee laajasti rauhallisesta aggressiiviseen ja tappavaan. On oleellista, että taudin luonne arvioidaan tarkasti, jotta vältytään sen liialliselta hoidolta, tinkimättä erinomaisista hoitotuloksista selviytymisessä ja elämän laadussa. Uudet kuvantamisteknologiat ja automaattityökalut mahdollistavat tämän.

Tämän väitöskirjan ensimmäisessä osatyössä oli tavoitteena arvioida anti-1-amino-3-$^{18}$F-fluorosyklobutaani-1-karboksyylihappo ($^{18}$F-FACBC) PET-tietokonetomografiaa (TT), PET-magneettiresonanssikuvantamista (MRI) ja multiparametrista MRI-kuvantamista (mpMRI) eturauhassyövän diagnoosivaiheessa. $^{18}$F-FACBC-kertymät olivat tilastollisesti merkitsevästi voimakkaampia korkean Gleason-luokituksen kasvaimissa, joten yhdistettyä PET-MRI-kuvantamista voidaan käyttää hyväksi esimerkiksi kohdennetussa koepalojen otossa. $^{18}$F-FACBC PET-MRI oli parempi kuin PET-TT ja samanveroinen kuin mpMRI eturauhassyövän diagnostiikassa. PET-MRI ja mpMRI eivät havainneet alle 8 mm:n läpimittaisia imusolmukemetastaaseja. $^{18}$F-FACBC PET-MRI on lupaava kuvantamismuoto eturauhassyövän diagnostiikassa, erityisesti kajoavia hoitoja suunniteltaessa, mutta ei korvanne mpMRI:a kliinisessä käytössä.

Toinen osatyö käsitteli luustoetäpesäkkeiden toteamista eri kuvantamismenetelmillä korkean uusiutumisriskin eturauhas- ja rintasyöpäpotilailla. Kaikille potilaille tehtiin $^{99m}$Tc-HDP luustokarttakuvaus, $^{99m}$Tc-HDP SPECT, $^{99m}$Tc-HDP SPECT-TT, $^{18}$F-NaF PET-TT ja koko kehon MRI diffuusiopainotettuna (wbMRI+DWI). $^{99m}$Tc-HDP SPECT-TT, $^{18}$F-NaF PET-TT ja wbMRI+DWI olivat perinteistä luustokarttaa herkempiä luustometastaasien toteamisessa, koska epäspesifeiksi määriteltyjä muutoksia oli vähemmän. wbMRI+DWI osoitti yhtäläistä tarkkuutta luustometastaasien diagnosoinnissa $^{18}$F-NaF PET-TT:n verrattuna, joten sitä voitaisiin hyödyntää, käytettäessä vain yhtä kuvantamistapaa näiden potilaiden luustometastaasien toteamiseen.

Kolmas osatyö arvioi ja validoi täysin automaattisen piirtotyökalun käyttöä MRI-pohjaisen sädehoidon suunnittelussa eturauhassyöpäpotilailla. Työkalu suoriutui hyvin eturauhasen, virtsarakon ja peräsuolen rajauksesta asiantuntijan käsin tekemiin rajauksiin verrattuna, puoltaen työkalun käyttöä luotettavasti myös kliinisessä työssä.

Viimeisenä, neljännessä osatyössä arvioitiin biologisesti ohjatun eturauhassyövän sädehoidon aiheuttamia pitkäaikaishaittoja. Hiili-11 asetaatti ($^{11}$C-ACE) PET-TT-kuvantamisen avulla suunniteltiin sädehoito, jossa metabolisesti aktiivisiin eturauhasen sisäisiin muutoksiin kohdistettiin korkeammat sädeannokset. $^{11}$C-ACE-PET-TT-ohjattu sädehoito oli toteuttamiskelpoinen ja hyvin siedetty. Vaikka erektiohäiriöt olivat suhteellisen yleisiä, vakavat suoliston haittavaikutukset olivat hyvin harvinaisia, eikä kolmannen asteen virtsateiden haittavaikutuksia esiintynyt lainkaan viiden vuoden kuluttua sädehoidosta.

Tämän väitöskirjan löydökset voivat parantaa eturauhassyövän primaaridiagnostiikan kuvantamista ja sädehoidon suunnittelua, sekä luustoetäpesäkkeiden diagnostiikkaa. Näin voidaan kohentaa potilaiden elämänlaatua ja selviytymistä.

AVAINSANAT: Eturauhassyöpä, magneettikuvaus, positroniemissiotomografia, sädehoidon suunnittelu, haittavaikutukset, luuston etäpesäkkeet

# Table of Contents

# Abbreviations

| | |
|---|---|
| $^{11}$C-ACE | $^{11}$C-acetate |
| $^{18}$F-NaF | $^{18}$F-sodium fluoride |
| 3D | three-dimensional |
| $^{99m}$Tc-HDP | $^{99m}$Technetium oxidronate |
| $^{99m}$Tc-MDP | $^{99m}$Technetium methylene diphosphonateADC apparent diffusion coefficient |
| AST | automatic segmentation tool |
| AUC | area under the ROC curve |
| AVD | absolute volume difference |
| BC | breast cancer |
| BPH | benign prostate hyperplasia |
| BS | bone scintigraphy |
| BVC | best valuable comparator |
| CAB | complete androgen blockade |
| CI | confidence interval (in the original article number III, also clinical investigator) |
| CMS | centre of mass shift |
| CT | computed tomography |
| DR | detection rate |
| DRE | digital rectal examination |
| DSC | dice similarity coefficient |
| DVH | dose volume histogram |
| DWI | diffusion weighted imaging |
| EBRT | external beam radiotherapy |
| EPE | extra prostatic extension |
| FOV | field of view |
| $HD_{95}$ | Hausdorff distance |
| IGRT | image guided radiotherapy |
| IMRT | intensity modulated radiotherapy |
| IPSS | international prostate symptom score |
| LEHR | low-energy high-resolution (collimator) |

| | |
|---|---|
| LHRH | luteinizing hormone-releasing hormone |
| LVI | lympho-vascular invasion |
| MRI | magnetic resonance imaging |
| OAR | organs at risk |
| PC | prostate cancer |
| PET | positron emission tomography |
| ROC | receiver operation characteristic |
| RTOG | Radiation Therapy Oncology Group |
| RTP | radiotherapy planning |
| sCT | synthetic computed tomography |
| SD | standard deviation |
| SI | signal intensity |
| SIB | simultaneous integrated boost |
| SPECT | single photon emission computed tomography |
| STIR | short tau inversion recovery |
| SV | seminal vesicles |
| T1w | T1-weighted |
| T2w | T2-weighted |
| TPS | treatment planning system |
| TR/TE | repetition time/echo time |
| TRUS | transrectal ultrasound |
| ULN | upper limit of normal |
| $V_T$ | distribution volume |
| wbMRI | whole-body magnetic resonance imaging |
| WHO | World Health Organization |

# List of Original Publications

This dissertation is based on the following original publications, which are referred to in the text by their Roman numerals:

I Ivan Jambor, Anna Kuisma, Esa Kähkönen, Jukka Kemppainen, Harri Merisaari, Olli Eskola, Jarmo Teuho, Ileana Montoya Perez, Marko Pesola, Hannu J. Aronen, Peter J. Boström, Pekka Taimen, Heikki Minn. Prospective evaluation of $^{18}$F-FACBC PET/CT and PET/MRI versus multiparametric MRI in intermediate- to high-risk prostate cancer patients (FLUCIPRO trial). Eur J Nucl Med Mol Imaging (2018) 45:355-364.

II Ivan Jambor, Anna Kuisma, Susan Ramadan, Riikka Huovinen, Minna Sandell, Sami Kanjander, Jukka Kemppainen, Esa Kauppila, Joakim Auren, Harri Merisaari, Jani Saunavaara, Tommi Noponen, Heikki Minn, Hannu J. Aronen & Marko Seppänen. Prospective evaluation of planar bone scintigraphy SPECT, SPECT/CT, $^{18}$F-NaF PET/ CT and whole body 1.5T MRI, including, DWI for the detection of bone metastases in high risk breast and prostate cancer patients: SKELETA clinical trial. Acta Oncologica (2016) 55:59-67.

III Anna Kuisma, Iiro Ranta, Jani Keyriläinen, Sami Suilamo, Pauliina Wright, Marko Pesola, Lizette Warner, Eliisa Löyttyniemi, Heikki Minn. Validation of automated magnetic resonance image segmentation for radiation therapy planning in prostate cancer. Physics and Imaging in Radiation Oncology (2020) 13:14-20.

IV Anna Kuisma, Pauliina Wright, Sami Suilamo, Jan Seppälä, Mari Koivisto, Paula Lindholm & Heikki Minn (2022) Long-term outcome of biologically guided dose-escalated radiotherapy of localized prostate cancer, ActaOncologica, 61:1, 97-103.

# 1 Introduction

Multiparametric magnetic resonance imaging (mpMRI) has shown good pooled sensitivity in detecting and localizing higher grade prostate cancer (PC) according to Cochrane meta-analysis (Drost et al., 2019). However, it is less sensitive to identify lower grade PC. Therefore, more advanced techniques are needed to improve non-invasive detection of PC. A hybrid imaging with combination of functional and anatomical information could help to characterize the benign lesions from cancer lesions. Different tracers have been studied in PC, e.g., tracers depicting lipid metabolism, such as $^{11}$C-acetate. Many cancers, including PC, have upregulated amino acid transport related to their proliferative potential (Huang & Mcconathy, 2013). The synthetic non-metabolized leucine derivate anti-1-amino-3-$^{18}$F-fluorocyclobutane-1-carboxylic acid ($^{18}$F-FACBC or $^{18}$F-fluciclovine) accumulates in PC (Schuster et al., 2013), but also in benign prostate hyperplasia (BPH) (Turkbey et al., 2014a) and needs therefore further studies. Assessment of metastasis often requires multiple imaging modalities due to equivocal findings that need to be re-evaluated.

MRI has also been progressively used in prostate cancer radiotherapy planning (RTP) (Schmidt & Payne, 2015), also as the sole imaging modality. Since the manual segmentation of organs at risk (OAR) can be highly work and time consuming, there is an abundant need to develop and validate automated segmentation tools (AST).

Several prospective randomized studies have shown that dose escalation in radiotherapy (RT) of localized PC improves biochemical control rate (Viani et al., 2009). Nevertheless, it is not acceptable to increase side effects of RT. We nowadays use modern technology, such as intensity modulated and image guided radiotherapy (IMRT/IGRT). With these technologies dose escalation of primary tumor may be possible without increasing the radiation dose of OARs. This requires multimodal imaging instead of conventional computed tomography (CT), which cannot depict tumor foci within the prostate gland (Chen ME et al., 2000).

The focus of this study was to compare different imaging modalities in distinguishing prostate cancer and its metastases. In addition, automatic segmentation tool in the radiotherapy planning of prostate cancer was validated and toxicity of dose-escalated prostate cancer radiotherapy was assessed.

# 2 Review of the Literature

## 2.1 Anatomy of the prostate gland

The prostate gland is located posterior to symphysis pubis, anterior to the rectum, and inferior the urinary bladder. The shape of the gland is like an inverted cone and it surrounds the proximal urethra, with its base attached to the neck of bladder and its apex resting on the superior surface of the urogenital diaphragma. The prostate gland is composed of glandular, stromal, muscular, fibrous, elastic, nerve, lymphatic, and vascular tissue (Lee et al., 2011).

The prostate gland divides into three anatomical zones based on histologically different zones: 1) the central zone (CZ) forms the base of the gland containing the ejaculatory ducts and approximately 25% of normal prostate volume; 2) the peripheral zone (PZ) is the largest zone, composing 70% of the gland and being the origin of PCa in 70% of the cases; 3) the transition zone (TZ) surrounds the urethra, consists of more fibromuscular tissue, and forms only 5% of the prostatic volume. The anterior fibromuscular stroma (AS) contains mostly muscular and fibrous tissue, not glandular tissue, in prostatic apex. The prostate is surrounded by a thin fibrotic pseudocapsule (Fig 1). In clinical praxis prostate is often divided into basis, midgland, and apex, or simply to left and right lobe.

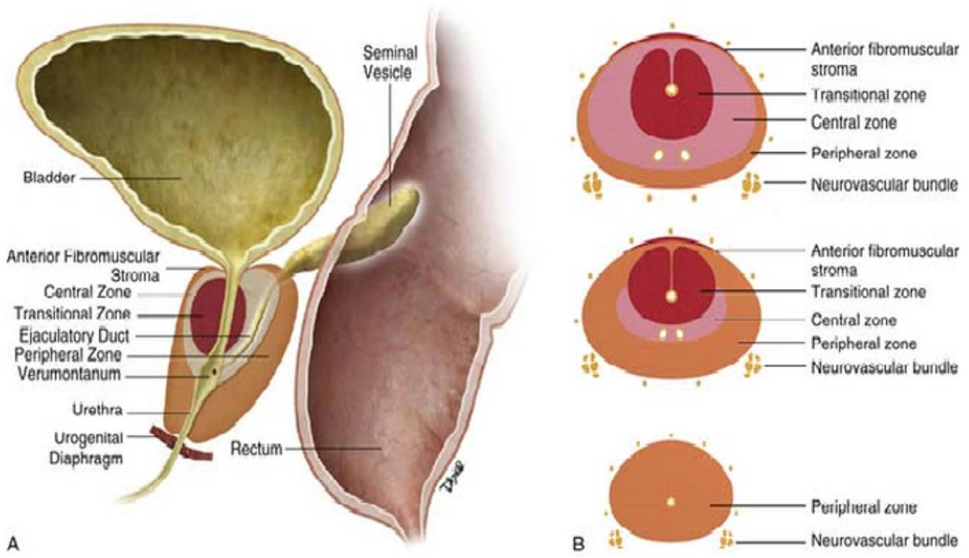


**Figure 1.** Prostate gland anatomy: A Sagittal view. B Axial view: top, base; middle, midgland; bottom, apex. Reprint with permission from radiologykey.com

## 2.2 Incidence and mortality of prostate cancer

Prostate cancer was the second most diagnosed cancer among men worldwide in 2020, with an estimated 1.4 million new cases and 375 000 deaths a year (Sung et al., 2021). In Finland, prostate cancer is the most common cancer in men with 5245 new cases diagnosed in 2019, representing 29 % of all cancer diagnoses in male population (*Cancer in Finland - Syöpärekisteri*, 2020). The prostate cancer-specific mortality was 934, accounting for 13 % of all cancer-related deaths in Finnish men. According to autopsy studies, the prevalence of PC increases with each decade of age in a nonlinear fashion from 5 % at age < 30 years to 59% by age >79 years (Bell et al., 2015).

## 2.3 Classification and staging

The aim of a tumour classification system is to combine patients with a similar clinical outcome. In the European Association of Urology (EAU) guidelines for prostate cancer (Mottet et al, 2020) the Tumour, Node, Metastases (TNM) classification for staging of PC is used (Table 1) (Brierley et al., 2016). The EAU risk group classification is based on D'Amico's classification system for PC, which groups the patients with similar risk of biochemical recurrence after radical prostatectomy (RP) or external beam radiotherapy (EBRT) (Table 2) (D'amico et al., 1998).

Gleason score (GS) consists of the most extensive (primary) pattern and the second most common (secondary) pattern of PC in prostate biopsies or the whole removed prostate. A GS≤5 should not be given based on prostate biopsies. The International Society of Urological Pathology (ISUP) grades the PC into five different categories (1–5) according to GS: ISUP grade 1 including GS 2–6, ISUP grade 2 including GS 7(3+4), ISUP grade 3 including GS 7(4+3), ISUP 4 including GS 8, and ISUP 5 including Gleason scores 9–10, respectively. (Epstein et al., 2016)

### 2.3.1 Histopathology of prostate cancer

Diagnosis of PC is based on histology. It is recommended to obtain 8–12 biopsies of prostate, number of biopsies depending on the size of the gland. The samples should be collected bilaterally from apex to base, additional biopsies should be targeted to suspected areas identified by digital rectal examination (DRE), transrectal ultrasound (TRUS), or mpMRI. It is mandatory to report the following elements for a carcinoma-positive prostate biopsy: type of carcinoma, primary and secondary or worst Gleason grade, percentage of carcinoma, ISUP grade, and, if identified, EPE (extraprostatic extension), LVI (lymphovascular invasion), and intraductal carcinoma. Histopathological examination after radical prostatectomy includes also the pathological stage and surgical margins of PC.

**Table 1.** The Clinical TNM Classification of prostate cancer.

| T | PRIMARY TUMOUR (STAGE BASED ON DIGITAL RECTAL EXAMINATION [DRE] ONLY) |
|---|---|
| **TX** | Primary tumor cannot be assessed |
| **T0** | No evidence of primary tumor |
| **T1** | Clinically inapparent tumor that is not palpable |
| **T1A** | Tumor incidental histological finding in 5% or less of tissue resected |
| **T1B** | Tumor incidental histological finding in more than 5% of tissue resected |
| **T1C** | Tumor identified by needle biopsy (e.g. because of elevated PSA[1]) |
| **T2** | Tumor that is palpable and confined within prostate |
| **T2A** | Tumor involves one half of one lobe or less |
| **T2B** | Tumor involves more than half of one lobe, but not both lobes |
| **T2C** | Tumor involves both lobes |
| **T3** | Tumor extends through the prostatic capsule |
| **T3A** | Extracapsular extension (unilateral or bilateral) |
| **T3B** | Tumor invades seminal vesicle(s) |
| **T4** | Tumor is fixed or invades adjacent structures other than seminal vesicles: external sphincter, rectum, levator muscles and/or pelvic wall |
| **N** | regional (pelvic) lymph nodes[2] |
| **NX** | Regional lymph nodes cannot be assessed |
| **N0** | No regional lymph node metastases |
| **N1** | Regional lymph node metastases |
| **M** | distant metastases [3] |
| **M0** | No distant metastases |
| **M1** | Distant metastases |
| **M1A** | Non-regional lymph node(s) |
| **M1B** | Bone(s) |
| **M1C** | Other site(s) |

[1] PSA= Prostate Specific Antigen

[2] Metastases no larger than 0.2 cm can be designated as micrometastasis (pNmi).

[3] When more than one site of metastases is present, the most advanced category is used. (p)M1C is the most advanced category.

**Table 2.** European Association of Urology (EAU) risk group classification for biochemical recurrence and locally advanced prostate cancer.

| LOW-RISK | INTERMEDIATE-RISK | HIGH-RISK | HIGH-RISK |
|---|---|---|---|
| PSA < 10 NG/ML | PSA 10-20 ng/ml | PSA >20 ng/ml | Any PSA |
| AND GS <7 (ISUP G I) | or GS 7 (ISUP G 2/3) | or GS >7 (ISUP G4/5) | Any GS (any ISUP Grade) |
| AND CT1-2A | or cT2b | or cT2c | cT3-4 or N+ |
| LOCALISED | Localized | Localized | Locally advanced |

GS=Gleason score, PSA= prostate specific antigen

### 2.3.2 Screening, Detection, and diagnostics of prostate cancer

The screening of PC is evaluated in the Cochrane review by Ilic et al. (2013). According to this review, the screening increases the number of diagnoses of PC but it reveals more localized disease than advanced PC. Furthermore, there were no PC-specific survival or OS benefit in the results (Ilic et al., 2013; Hayes & Barry, 2014). Therefore, the screening for PC is only recommended if the patients are well informed on the risks and benefits of the testing, and they are at elevated risk of having PC (age >50 years, or age >45 years with family history of PC or African descent, or age >40 years in men carrying BRCA2 mutation). About 9–20% of PC patients have true hereditary disease but it is associated with a 6–7-year earlier disease onset (Hemminki, 2012). Anyhow, the disease aggressiviness and clinical behavior does not seem to be different in other ways.

Elevated PSA levels or suspicious finding in DRE are the most usual reasons to suspect PC and begin further diagnostical examinations.
Since most PCs are in the peripheral zone, part of them can be detected by DRE. Definitive diagnosis is confirmed with systematic TRUS-guided biopsy. Prostate-spesific antigen (PSA) is a specific marker for prostate gland but not for PC (Stamey, 1987). It increases typically in PC but also in benign diseases such as benign prostate hyperplasia (BPH) and infections of prostate and bladder. There is no absolute PSA threshold for diagnosis of PC, but since PSA is a continuous parameter, higher levels depict higher probability of PC (Stamey et al., 1987). Absolute annual increase in serum PSA (PSA velocity) and PSA doubling time (PSA-DT) have been evaluated to measure the aggressivity of PC. Free/total PSA ratio can be used in men with PSA 4–10 ng/ml to predict the likelihood of PC but has no use in follow-up or higher PSA levels (Y. Huang et al., 2018).

#### 2.3.2.1 Diagnostics

The base of the diagnostics in PC is TRUS-guided biopsy, which can be performed transrectally or transperineally. Multiparametric magnetic resonance imaging (mpMRI) has good sensitivity (0.91, 95% CI: 0.83-0.95) and specificity (0.37, 95% CI: 0.29-0.46) for identifying of ISUP grade ≥2 PC, but less sensitive and specific in detecting ISUP grade 1 PC (Drost et al., 2019).

The extent of PC is assessed by DRE and PSA measurement and may be supplemented with mpMRI, bone scintigraphy, and computed tomography (CT).
Before surgery, PC patients typically undergo CT and/or MRI for lymph node staging. However, both modalities only detect nodal metastases if the nodes are enlarged, their sensitivity ranging between 39 and 42% (Hövels et al., 2008).

## 2.4 Primary treatment

This chapter introduces the major contemporary treatment approaches for PC (Thomsen et al., 2014), including active surveillance, surgery, and radiotherapy. The ProtecT trial (Hamdy et al., 2016) evaluated the 10-year outcomes of 1643 patients after active monitoring, surgery, or radiotherapy for localized PC, demonstrating equal PC-specific survival rates for all treatment options (98.8%, 99.0%, and 99.6%, respectively). Surgery and RT were associated with lower incidence of progressive and metastatic disease than active monitoring.

### 2.4.1 Active surveillance

In localized PC, low-risk and selected intermediate-risk PC patients with life-expectancy of >10 years, active surveillance can be chosen to avoid unnecessary treatment and side effects. Patients remain under regular follow-up, and curative treatment is initiated immediately, when predefined thresholds indicate a progression in the disease. Thomsen et al. reviewed 10 studies of active surveillance (including 3550 patients), concluding it to reduce over-treatment without compromising 10-year PC-specific survival, reaching 96-100% in both risk groups (Thomsen, 2014).

### 2.4.2 Surgery

Prostatectomy can be performed by open, laparoscopic, or robot-assisted approaches (Ilic et al., 2017). According to Cochrane review (Ilic et al., 2013), there is no high-quality evidence to compare effectiveness of these three surgical treatment techniques for oncological outcomes. Urinary and sexual quality of life appeared similar, as well as overall and serious postoperative complication rates. Performing a pelvic lymphadenectomy during prostatectomy provides essential information for staging and prognosis but does not improve oncological outcomes and may cause more perioperative and postoperative complications (Fossati et al., 2017).

### 2.4.3 Radiotherapy

The current standard techniques in RT of PC are intensity modulated and image guided radiotherapy (IMRT/IGRT), where a uniform dose is delivered to whole prostate, limited by the tolerance of OARs, bladder and rectum (Mottet et al., 2017; Zelefsky et al., 2008). Local recurrences typically occur in the site of the primary tumor, indicating that dose escalation in the primary lesion rather than the whole prostate gland has possibility to improve disease control without raising toxicity (Cellini et al., 2002). Biochemical control rate of localized PC has been improved by dose-escalated RT (range 74–80 Gy) in several prospective randomized studies

(Viani et al., 2009). Microscopic spread of PC is typically multifocal, not discovered by CT, therefore this strategy requires advanced multimodality imaging, including MRI or PET/CT (Chen et al., 2000). PC has a slow proliferation rate and is therefore affected more by hypofractionated RT (2.5-4 Gy/fr) than conventional fractions (1.8–2.0Gy/fr) (Dasu & Toma-Dasu, 2012). Hypofractionated RT offers also the advantage of shorter treatment period, saving patients from the inconvenience of long treatment periods and diminishing the costs.

#### 2.4.3.1.1 Prostate delineation in PC RTP

Advances in imaging and technology in last decades have improved the target coverage and normal tissue sparing in radiotherapy treatment delivery. However, sharp dose gradients are a benefit only, if the geometric uncertainty in delineation is small (Njeh, 2008). The use of MR alone or together with CT improves the accuracy e.g. in PC RTP (Rasch et al., 2005) and is increasingly used in it. Nyholm & al. evaluated the intra- and inter-physician variability of prostate and seminal vesicle (SV) delineations in RTP MRsequences. The variation in intra-physician SV delineation was significantly greater than the prostate delineation, thus inter-physician variability was similar in both organs. (Nyholm et al., 2013). Delineation has been considered as the weakest link in accuracy of RT (Njeh,2008). Automatic segmentation tools (AST) for RTP has been developed, ranging from adaptive thresholding to atlas-based techniques (Sharp et al., 2014), and more recently shifting towards artificial-intelligence-based methods (LeCun et al., 2015). Kiljunen et al. evaluated accuracy and efficiency gain of AST for CT in PC patients. The mean Dice similarity coefficient (DSC) between manual and automatic contouring were 0.82 for prostate, 0.72 for SV, 0.93 for bladder, and 0.51 for penile bulb, proving that using a general deep-learning-based AST for CT images saves time and improves consistency (Kiljunen et al., 2020).

### 2.4.3.2 Side effects of RT

The most typical side effects after PC RT are genito-urethral (GU) and gastro-intestinal (GI) symptoms. The side effects may be acute (<3 months) or late (>3 months) after RT. GU symptoms include nocturia, pollacisuria and very seldomly urinary retention or haematouria. GI symptoms include loose tools, diarrhea, and very rarely bleeding haemorrhoids or radiation proctitis. (Wang et al., 2020). Acute side-effects are more common than late ones (grade 1–3 GU toxicity in 50% and grade 1-3 GI toxicity in 30% of patients in EORTC 22991 trial) but they tend to resolve by time (Matzinger et al., 2009). When IMRT and IGRT are used for dose

escalation (74–80Gy), rates of severe late side effects (≥ grade 3) for rectum are 2–3% and for the GU tract 2-5% (Viani et al., 2009).

### 2.4.4 Hormonal therapy, chemotherapy, radionuclide treatment

Androgen deprivation can be obtained by either suppressing the secretion of testicular androgen or inhibiting the action of circulating androgens at the receptor level. The first can be achieved by bilateral orchiectomy or long-acting luteinizing hormone-releasing hormone (LHRH) agonist injections, the latter by LHRH antagonist injections or steroidal and nonsteroidal oral anti-androgens (e.g., bicalutamide). To reach complete androgen blockade (CAB), LHRH-agonist/antagonist and bicalutamide can be combined. These hormonal treatments can be used as a monotherapy, neo-adjuvant or adjuvant therapy, together with RP or EBRT at first line, treating intermediate or high-risk PC. They are also used in metastatic PC and can be delivered continuously or intermittently (Mottet et al., 2017).

All the PC patients with ADT develop castration resistance over time; several new compounds have been developed to target the androgen axis. These drugs (e.g., enzalutamide, abiraterone acetate) aim to diminish the symptoms related to PC and increase the quality of life. Aminobisphophonates (zoledrone acid, ibandronate and denosumab) inhibit pathological fractures and prolong the time to progression. Docetaxel chemotherapy can be delivered at early phase in primarily metastatic PC, or later after castration resistance. Cabazitaxel is typically used in second line. Radium-223 dichloride, an alpha emitter selectively targeting bone metastasis with alpha particles, has been shown to improve overall survival and prolong the time to the first symptomatic skeletal event in prostate cancer (Parker et al., 2013). The increasing utility of PSMA PET has enabled the use of lutetium-177-PSMA in radioligand therapy, which has been reviewed in meta-analysis and suggested to be effective treatment with low toxicity in metastatic state of castration-resistant PC (Yadav et al., 2019).

## 2.5 Metastases

Although local and adjuvant treatments have advanced, approximately 15–20% of patients will relapse, and 70% of these will later develop bone metastases. The most common sites for PC metastases are lymph nodes and bones. Hence, imaging techniques identifying early metastatic bone lesions are required to accurately stage men with intermediate or high-risk PC. Bone metastases are considered as a serious complication of cancer, causing pain, pathological fractures, spinal cord and other

nerve-compression syndromes. Bone metastasis are typically osteoblastic, sclerotic, or mixed lesions containing both elements, in PC predominantly osteoblastic. (Roodman, 2004).

## 2.6 Anatomical and functional imaging

It is crucial to depict primary TNM staging right in high-risk and intermediate-risk PC patients to be able to offer the optimal oncological benefit of treatment. Nearly all currently available PC risk nomograms depend on Gleason score and/or tumor volume for appropriate risk stratification. Therefore, it is also important to have highly sensitive and specific, accurate and reliable imaging modalities to detect primary tumors and metastases in PC. The disease spreading to regional lymph nodes is a well-known prognostic factor, although the therapeutic role of pelvic lymph node dissection during prostatectomy remains controversial (Fossati et al., 2017).

Traditionally, primary staging of lymph nodes is carried out using CT or MRI, relying on changes in size and morphology of lymph nodes. However, 80% of the metastatic lymph nodes are smaller the threshold limit of 8 mm, which is usually used in clinical practice (Hövels et al., 2008). Thus, there is demanding need for more sensitive lymph nodes staging in primary phase of high-risk PC. Previous data from meta-analysis of CT and MRI imaging reports sensitivity of 39–42% and specificity of 82%. (Hövels et al. 2008).

### 2.6.1 Bone scintigraphy and SPECT/CT

The current and most widely accepted modality to assess the distant bone metastases in PC is bone scintigraphy (BS). A planar γ-camera scan is performed after injection of technetium-99m-labeled methylene diphosphonate ($^{99m}$Tc-MDP), aiming to detect $^{99m}$Tc-MDP attached to active bone-remodeling sites (Ulmert et al., 2015). Unfortunately, combined sensitivity and specificity for BS at a lesion level is only 59% (95% CI: 55-63%) and 75% (95% CI: 71-79%), respectively, as shown in a recent meta-analysis (Shen et al., 2014). A similar modality, single-photon emission computed tomography (SPECT), gathers volumetric information on distribution of the $^{99m}$Tc-MDP by rotating γ-detectors around the patient during imaging. SPECT has proven its superiority compared with BS; combined sensitivity and specificity for SPECT at a lesion level is 90% (95% CI: 86-93%) and 85% (95% CI: 80-90%), respectively. (Shen et al., 2014).

## 2.6.2 Positron emission tomography (PET)

Positron emission tomography (PET) is a molecular imaging modality which uses short-lived isotopes to depict accurate information on body function, metabolism, and biology. Today, all PET is performed as hybrid imaging combining with computed tomography (CT) or MRI device, providing both functional (PET) and anatomical (CT or MRI) information of the body.

### 2.6.2.1 PET tracers

PET is nowadays routinely used for diagnosis, staging, and therapy follow-up in oncology. However, the general-purpose tracer $^{18}$F-fluoro-2-deoxy-D-gluocose (FDG) low detection rate of PC due to limited glucose uptake, especially in patients with low or intermediate Gleason score. However, poorly differentiated PC can be visualized variably with FDG PET. Various PET tracers have been evaluated in numerous systematic reviews and meta-analyses in the imaging of PC recurrence (Evans et al., 2018; Schuster et al., 2016). Cautious interpretation of different sensitivity and specificity values is recommended due to lacking histological confirmation of imaging findings in most of the trials.

#### 2.6.2.1.1 18F-NaF

$^{18}$F-sodium fluoride ($^{18}$F-NaF) PET/CT is very sensitive in detecting osteoblastic lesions and is therefore considered especially useful in staging and identification of early bone metastases in PC. Despite the nonspecific nature of $^{18}$F-NaF PET/CT, it reaches high specificity in revealing bone metastases but lacks the ability to distinguish primary cancer in prostate gland and local and distant nodal disease.

#### 2.6.2.1.2 $^{11}$C or $^{18}$F Choline

$^{11}$C or $^{18}$F Choline PET/CT has been evaluated in meta-analysis by von Eyben and Kairemo (2014). PC is associated with high uptake of choline and involves high levels of choline kinases and choline transporters, allowing higher detection rate, also in early tumor infiltration of bone marrow. Meta-analysis indicated that choline has advantages compared to bone scintigraphy and $^{18}$F-FDG PET/CT. A positive finding in BS represented a reaction in bone formation, while positive choline PET/CT reflected tumor cells. $^{11}$C or $^{18}$F Choline PET/CT is considered to be useful as the first imaging method for patients with PC and biochemical recurrence with PSA levels from 1.0 to 50 ng/ml, indicating local, regional or distant disease in most patients. However, the pooled sensitivity of choline PET/CT for pelvic LNs was only

0.62 (CI 0.51-0.66), reaching only moderate diagnostic accuracy (von Eyben & Kairemo, 2014).

#### 2.6.2.1.3 $^{11}$C acetate

Carbon-11-labeled acetate tracer ($^{11}$C-ACE) has minimal accumulation in the urinary bladder, which enables optimal assessment of the pelvic disease and prostatic gland. Encouraging results have been reported by Jambor et al. (Jambor et al., 2010), $^{11}$C-ACE PET/CT showing sensitivity, specificity, and accuracy of 88%, 41%, 74%, respectively, when evaluating intraprostatic tumors. Yet, most investigators would agree, that the specificity of $^{11}$C-ACE PET/CT is relatively low and probably not worthwhile for the evaluation of the prostatic tumors while MRI is preferable (Jambor et al., 2012a).

The tracer has also been studied in PC patients for lymph nodal staging undergoing radical prostatectomy (Schumacher et al. 2015). Schumacher et al. reported nodal-region-based sensitivity, specificity, positive predictive value, and negative predictive value of 62%, 89%, 62%, and 89%, respectively. Other studies have shown similar results, indicating $^{11}$C-ACE to be suboptimal tracer for nodal staging in primary PC.

The $^{11}$C-ACE has also been tested for recurrent PC and some trials have indicated $^{11}$C-ACE PET/CT may be useful in the early evaluation of PC relapse (Albrecht et al., 2007). However, the results in different studies have been discrepant.

Currently, there is no conclusion on an issue which one of these radiotracers, either choline or acetate, would be superior in PC lesion detection. They both have insufficient accuracy in evaluation of primary PC and are not able to differentiate cancer from benign lesion within the prostate gland. The PSA level influences the sensitivity of both tracers in staging the recurrent disease and is recommended to be >2 ng/ml.

#### 2.6.2.1.4 Fluciclovine (FACBC)

One of the most investigated non-natural amino acid tracers is anti-1-amino-3-$^{18}$F-fluorocyclobutane-1-carboxylic acid (FACBC or fluciclovine). It has many advantages compared with natural amino acid radiotracers, including easier synthesis, the ability to radiolabel with long live radionuclides, and simplified kinetics (C. Huang & Mcconathy, 2013). The feasibility of fluciclovine has been reported in staging of primary and metastatic PC (Sörensen et al., 2013). In recurrent PC, sensitivity, specificity, and accuracy of fluciclovine PET/CT was 90.2%, 40.0%, and 73.6%, respectively (Schuster et al., 2014). Fluciclovine has shown superior performance when compared with choline, detecting higher number of true positive

and true negative lesions in the prostate bed, lymph nodes, and bone (Nanni et al., 2016).

#### 2.6.2.1.5 PSMA

Prostate-specific membrane antigen (PSMA) is a trans-membrane protein expressed in the epithelial cells surrounding prostatic ducts (DeMarzo et al., 2003). PSMA is over-expressed in most PC cells within the prostate and LN metastases (Sweat et al., 1998) In the primary tumors of PC, the GS and PSA level correlate with the $^{68}$Ga-PSMA-11 accumulation (Uprimny et al., 2017). $^{68}$Ga-PSMA PET studies have been reviewed by Corfield et al. (Corfield et al., 2018), results concluding lesion-based sensitivity of 33–92%, and median lesion-based specificity ranging from 82-100 in primary staging of PC (Koschel et al., 2019). $^{68}$Ga-PSMA-11 PET-CT provided superior accuracy when compared with conventional imaging (CT and BS) by Hofman et al. (Hofman et al., 2020). They reported accuracy of 92% (88–95) for PSMA PET and 65% (60-69) for conventional imaging, respectively ($p<0.0001$), in a prospective, randomized study in high-risk PC patients before treatment. The accuracy of PSMA-PET was also higher than of conventional imaging for pelvic LN metastasis (AUC 91% vs 59 %), and distant metastasis 95% vs 74%. Radiation exposure was lower for PSMA-PET-CT than conventional imaging (8.4 mSv vs 19.2 mSv, $p<0.001$).

$^{18}$F-PSMA and $^{68}$Ga-PSMA PET/CT have similarly showed good detection rates (DR) in recurrent PC (Treglia et al., 2019), the pooled detection rate of $^{18}$F-PSMA was 81% (95% CI 71-88%). The detection rate of $^{18}$F-PSMA was related to PSA value, pooled DR being 86% for patients with PSA ≥0.5 ng/ml (95% CI 78-93%) and 49% (95% CI 23-74%) with PSA <0.5 ng/ml. In evaluating recurrent disease, PSMA-PET detection rate was related to the level of PSA also according to Perera et al. (2016). The pooled estimate for PSMA positivity was 42% at a PSA level of < 0.2 ng/ml and 95% with PSA level >2.00 ng/ml. The pooled PSMA positivity was 92% for PSA doubling time (PSAdt) of < 6 months and 64% for ≥ 6 months.

Although novel imaging modalities and new tracers have been developed, a significant increase in the usage of PET only occurred following the introduction of PSMA, due to its limited sensitivity to detect lymph node metastases in low PSA values with other novel PET tracers.

### 2.6.3 MRI

MRI has a superior soft tissue contrast and is therefore increasingly used in PC RTP for target and normal structure delineation (Schmidt & Payne, 2015). Diffusion weighted imaging is a functional imaging technique that measures the random

motion of water molecules within the intravascular, intracellular, and extracellular compartments. The free diffusion of water is impeded by cell membrane integrity and different cellularities, which can be utilized to characterize biological tissues (Qayyum, 2009).

Prostate Imaging and Reporting Data System (PI-RADS) was initially introduced in 2012 by the European Society of Urogenital Radiology (Bomers & Barentsz, 2014). The updated version emphasizes the use of certain sequences when evaluating specific zones of the prostate. The suspected cancer lesions are scored by a 5-point scale stratified by three pulse sequences: T2 weighted imaging (T2WI), diffusion weighted imaging (DWI), and dynamic contrast-enhanced (DCE). PI-RADS version2 is widely accepted as the global standard scoring system when reporting mpMRI findings in the prostate gland (Schimmöller et al., 2013).

# 3 Aims

The aims of this thesis were to a) compare different imaging modalities in detection the prostate cancer and its metastases, and b) to validate an automatic segmentation tool in the radiotherapy planning of prostate cancer and evaluate the toxicity of dose-escalated prostate cancer radiotherapy. The specific aims of the sub-studies were:

1. To compare the effectiveness of $^{18}$F-FACBC PET/CT, PET/MRI, and mpMRI in the discovery and characterize of primary tumors and pelvic lymph nodes in prostate cancer patients about to undergo robot-assisted radical prostatectomy (FLUCIPRO).
2. To compare the accuracy $^{99m}$Tc-HDP BS, $^{99m}$Tc-HDP SPECT, $^{99m}$Tc-HDP SPECT/CT, $^{18F}$NaF PET/CT and whole-body 1.5 Tesla (T) MRI, including DWI (mpMRI+DWI), in diagnosing bone metastases in high-risk prostate cancer and breast cancer patients (SKELETA).
3. To evaluate and validate the performance of a fully automatic MRI segmentation tool used in radiotherapy planning of prostate cancer (AUTOCONTOURING).
4. To assess the late toxicity of biology-guided dose-escalated radiotherapy in prostate cancer patients (ACEPRO).

# 4 Materials and Methods

## 4.1 Patients

Patients with histologically confirmed prostate cancer (PC) diagnosed through systemic TRUS-guided biopsies, were enrolled in studies I-IV. Study II also included breast cancer (BC) patients with histologically confirmed diagnosis. Fiducial markers were placed in the prostate for all PC radiotherapy patients according to local clinical protocol. All the patients had to be able to understand the meaning of the study and were not to have serious uncontrolled infection, history of serious cardiovascular, liver of kidney disease, or contraindications for MRI (cardiac pacemaker, intracranial clips, hip prosthesis, claustrophobia). All four studies were conducted at Turku University Hospital in Finland and total of 174 patients were included in the analysis. The combined patient characteristics are seen in Table 3. The flowchart of all enrolled patients in these four studies is on (Figure 2).

In study I (FLUCIPRO), 32 PC patients scheduled for radical robot-assisted prostatectomy were prospectively enrolled. Inclusion criteria were age 50-85 years, no previous surgical, radiation, or endocrine treatment for PC, clinical stage T1c-T3aN0 based on TRUS, creatinine ≤1.5 x ULN (Upper Limit of Normal). Exclusion criteria also included patient's preference for active surveillance as a method of PC management. Six men could not undergo all the scans for logistical reasons or refusal to participate after signing approved informed consent. Thus, 26 patients underwent the planned imaging sessions and were included in the analysis.

In study II (SKELETA), 27 PC and 26 BC patients with high risk of bone metastases were registered if they met at least one of the following inclusion criteria: 1) bone metastases were highly suspected clinically: localized ache over bone area; 2) laboratory findings: raised alkaline phosphatases (>105 U/l), elevated PSA or high PSA doubling time after prostatectomy or radiotherapy; 3) histopathologic findings: stage T3a and/or higher and/or Gleason score 4+3 or higher in PC patients, stage N3a or higher in BC patients; 4) age 40-80 years, WHO performance status 0-2. Exclusion criteria included ongoing treatment for metastatic disease. All PC and BC patients underwent the assessment of possible bone metastases after prostatectomy/mastectomy and/or external radiotherapy.

In study III (AUTOCONTOURING), 87 consecutive PC patients referred to definitive prostate RT were enrolled in the study if they met the following inclusion criteria: newly diagnosed histologically confirmed local or locally advanced PC (clinical stage T1c-T3bN0-N1), age between 40-90; WHO performance status of 0-1 and no prior oncologic treatment except for 4 to 6 months of neoadjuvant anti-androgen therapy.

We found 87 patients matching the inclusion criteria. However, eight patients were excluded due to technical issues caused by either large amount of rectal air, hip prosthesis, or obesity of the patient, which caused the MRCAT algorithm failing to generate the syntheticCT (sCT) image correctly. Nine other patients had to be excluded due to partially missing image data required to produce the automatic organ delineations. The image data was partially lost during software update of the MR console, as some of the necessary image data had not been backed up, and the local image database was emptied during the software update for 5 patients. At the end, 65 patients were included in the analysis.

In study IV (ACEPRO), 39 PC patients referred to external beam RT were enrolled prospectively. Other inclusion criteria were age 50-85 years, no previous surgical, radiation, or endocrine therapy for PC, clinical stage T1c-T3aN0M0 based on transrectal ultrasound, pelvic CT/MRI and bone scintigraphy, serum creatinine $\leq$1.5 x ULN. Exclusion criteria included that patient must have no contraindications for endorectal coil. Three patients cancelled their participation after signing up the consent form. We excluded four patients with pelvic lymph node RT and two patients with no SIB. At the end 30 patients who had similar dose distributions in the IMRT were included in the analysis.

**Table 3.** Combined patient characteristics from studies I-IV.

| STUDY | NUMBER OF PATIENTS | MEDIAN AGE YEARS (SD, RANGE) | MEDIAN PSA (SD, RANGE) | HORMONAL THERAPY % (N/N TOTAL) | PROSTATE CA RISK GROUPS % (N/N TOTAL) LOW INTERMEDIATE HIGH |
|---|---|---|---|---|---|
| **I FLUCIPRO** | 26 | 65(49-76) | 12 (4.1-35) | 0 | 0% (0)<br>4% (1/26)<br>96% (25/26) |
| **II SKELETA** | 27 PC<br>26 BC | 67 (60-79)<br>61 (27-76) | 12 (1-140) | 48% (13/27)<br>58% (15/26) | All at high risk for bone metastases |
| **III AUTOCONTOURING** | 65 | 73 (51-83) | 10(1.7-85) | 91% (59/65) | 0% (0)<br>31% (20/65)<br>69% (45/65) |
| **IV ACEPRO** | 30 | 67 (58-78) | 8.2(1.4-16) | 0 | 17% (5/30)<br>57% (17/30)<br>26% (8/30) |

## 4.2 Ethical considerations

All of the studies were performed in accordance with the Declaration of Helsinki. The studies were approved by the Ethics Committee of Hospital District of Southwest Finland.

In studies I, III, and IV, all patients gave written informed consent. In study III, the informed consent was obtained from those 15 patients who underwent a second MRI for the repeatability sub-study. Because MRI is part of routine RTP workflow in PC at the performing institution, no consent was needed for patients receiving a single MRI.

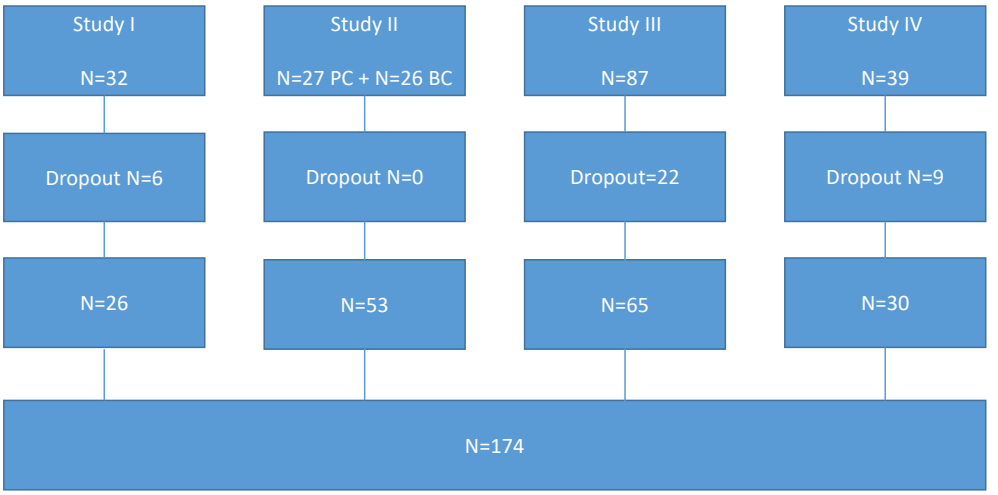


**Figure 2.** Flowchart of enrolled patients in the studies I-IV. Abbreviations: PC=prostate cancer, BC=breast cancer, N=number of patients.

## 4.3 Methods

In these four studies, several investigational methods were used. We used following imaging modalities: PET/CT, MRI, PET/MRI, BS, and SPECT/CT. Histopathological analysis in diagnosing PC or BC were used in studies I-IV according to international guidelines. In study I, the whole prostate gland was analyzed after prostatectomy, whereas in other studies only needle biopsies were performed and analyzed to confirm the diagnoses of PC. Additionally, in studies I and II visual evaluation of imaging was used, and in study I and III also quantitative analysis with different parameters were performed. Each study method is presented below, but if the same method has been used in more than one study the description is not repeated.

### 4.3.1 Methods of study I

In study I, PC patients underwent three different imaging modalities ($^{18}$F-FACBC PET/CT, $^{18}$F-FACBC PET/MRI, and multiparametric MRI) before robot-assisted prostatectomy. The methods used in this study were visual and quantitative evaluation and histopathological analysis. The study design of sturdy I is shown in Figure 3.

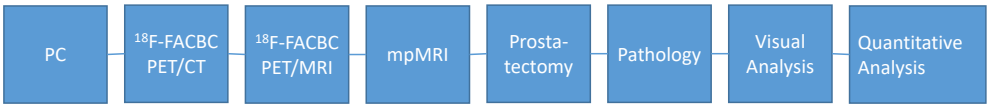


**Figure 3.** Study design of study I.

#### 4.3.1.1 $^{18}$F-FACBC PET/CT

In study I, $^{18}$F-FACBC PET/CT imaging data were acquired using a hybrid Discovery 690 PET/CT scanner (General Electric Medical Systems, Milwaukee, WI, USA) with a 64-slice CT and PET operated in 3-D mode. Inplane spatial resolution in PET was maximum of 4 mm full width at half-maximum (Bettinardi et al., 2011). All quantitative corrections applied to the PET sinogram data took into account detector dead time, radioactivity decay, random scatter, and photon attenuation. PET images were reconstructed in a 128 x128 matrix with a voxel size of 5.47 x 5.47 x 3.27 mm$^3$, using the VUE Point FX algorithm with time-of-flight. $^{18}$F-FACBC (fluciclovine) synthesis was performed by using a FASTlab™ Synthesizer (GE Healthcare, Waukesha, WI, USA) as the production module and the FASTlab cassettes (Ge Healthcare) and synthesis sequence designed for $^{18}$F-FACBC production.

Before imaging, each patient was asked to fast 4-6 hours and empty the rectum, but no enema was used. Each participant received an intravenous injection of 369 ± 10 MBq (mean ± SD) of $^{18}$F-FACBC diluted in 3-5 ml of saline as a 30-second bolus that was promptly flushed with saline. Emission imaging with the prostate in the center of the field of view was started immediately after the injection, preceded by pre-injection transmission imaging using low-dose CT. Following 20 min of dynamic data collection with a list-mode acquisition, additional table positions covering the whole pelvis and abdomen were acquired with 4-minute durations per position. The dynamic data were reconstructed to five frames with a frame time of 4 minutes.

#### 4.3.1.2 $^{18}$F-FACBC PET/MRI

In study I, following the PET/CT imaging, patients were transferred to PET/MRI suite housing the Ingenuity TF PET/MRI scanner (Philips Medical Systems, Cleveland, OH, USA). MR-based attenuation corrections were made to the PET data, taking into account detector dead time, radioactive decay, random scatter, and photon attenuation. PET images were reconstructed in a 144 x 144 matrix with an isotropic voxel size of 4 mm. PET/MRI studies were started with the attenuation correction in the MRI gantry, followed by a move to the PET gantry for PET imaging. Two table positions of 4 minutes each covering the whole pelvis were acquired. Finally, the patient table was moved back to the MRI gantry for acquiring MRI data. T2-weighted (T2w) images were obtained using a single-shot turbo spin-echo sequence followed by diffusion weighted imaging (DWI) with a single shot spin-echo-based sequence with a monopolar diffusion gradient scheme and echo-planar readout. DWI was performed as previously described using 12 b values (0, 100, 300, 500, 700, 900, 1100, 1300, 1500, 1700, 1900, 2000) (Jambor, et al.2016a; 2016b). Finally, T2w and DWI (performed using b values of 0 and 800 s/mm$^2$) covering the whole pelvis were obtained. Additional MR acquisitions were acquired (Jambor et al., 2015) but not evaluated in the current study.

#### 4.3.1.3 Multiparametric MRI

In study I, mpMRI was performed using a 3T MR scanner (Magnetom Verio 3 T, Siemens Healthcare, Erlangen, Germany) and surface array coils as previously described (Jambor et al., 2015). The imaging consisted of triplanar T2w turbo spin-echo imaging, single-shot spin-echo-based DWI and dynamic contrast inhanced (DCE) MRI. Two separate single-shot spin-echo-based DWI acquisitions were performed (Jambor et al., 2015) (Jambor et al., 2017) using 5 b values (0, 100, 200, 350, 500 s/mm$^2$) and 16 b values (0, 50, 100, 200, 350, 500, 650, 800, 950, 1100, 1250, 1400, 1550, 1700, 1850, 2000 s/mm$^2$) (Jambor et al., 2014).

#### 4.3.1.4 Visual evaluation

In study I, an experienced nuclear medicine physician and a co-worker PhD student interpreted the PET/CT images, aware of the PC diagnosis but not of other clinical and histopathological findings. A previously described region-based approach was used in visual evaluation of PET/CT (Kahkonen et al., 2013), leading to estimates of PC presence in 12 regions. Abnormal uptake was defined as any mono- or multifocal uptake greater than adjacent background in >1 slice within the CT-defined prostate gland area (Jambor et al., 2012b).

Multiparametric magnet resonance imaging was scored using a Likert system (Jambor et al., 2015; Rosenkrantz et al., 2013). Following trial completion, PI-RADs version 2 scores were added to the reports. mpMRI reporting was done in an anonymized random fashion blinded to PET/CT or PET/MR datasets.

The same readers visually evaluated PET/MRI in consensus using the same region-based analysis (Kahkonen et al., 2013), visualizing T2w, DWI (trace and parametric maps), and PET images simultaneously. Any mono- or multifocal uptake of $^{18}$F-FACBC originating from nodules of BPH identified on T2w and DWI was not considered to represent PC. Focal uptake in the central gland and peripheral zone beyond that of adjacent backround with no pathological changes on T2w and DWI or related to benign conditions was considered as a tumor focus (Jambor et al., 2012).

#### 4.3.1.5 Quantitive evaluation

In study I, logan plots (Logan, 2000) with a reference region in the iliac/femoral artery were used to estimate the tracer distribution volume ($V_T$) based on the assumption that transport of $^{18}$F-FACBC into cells is similar to reversible receptor binding kinetics (Turkbey et al., 2014b). DWI datasets were post-processed at a voxel level using monoexponential function (apparent diffusion coefficient, ADC).

#### 4.3.1.6 Histopathological analysis

In study I, whole-mount prostatectomy sections were prepared as described (Toivonen et al., 2015) and analyzed together by an experienced genitourinary pathologist. Whole-mount axial macrosections were obtained at 5 mm (range 4–6) intervals in plane perpendicular to the long axis of the prostate gland in a superior-inferior direction. The most apical and basal macro sections were further sectioned in coronal orientation for better evaluation of the capsular status at the inferior and superior regions. Subsequently, the tissues were embedded in paraffin using macro-cassettes and the histological sections were cut at 4 micrometers and stained with hematoxylin and eosin. The presence and location of cancer foci, high grade prostatic intraepithelial neoplasia, prostatitis, BPH, capsular status, and seminal vesicle invasion were determined. For each tumor focus, GS was assigned as a combination of primary, secondary and tertiary (when applicable) Gleason grade (Epstein et al., 2005). Tertiary Gleason grade was assigned only if a Gleason grade pattern higher than the primary and secondary, grades was present and the tertiary grade component was estimated visually to represent less than 5% of the tumor (Epstein, 2010). Tumors were classified into three groups: GS 3+3, 3+4, and >4+3, only. Only tumor foci >0.5 cm, largest lesion diameter, as defined using whole-mount prostatectomy sections, were included in analyses.

### 4.3.2 Methods of study II

The study design of study II is shown in Figure 4.

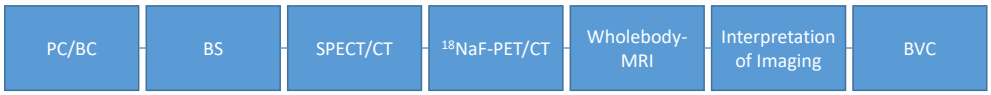


**Figure 4.** Study design of study II.

#### 4.3.2.1 Synthesis of NaF

The irradiated water containing $^{18F}$F is applicated on a pre-conditioned solid phase extraction cartridge (Accell Plus QMA, light, Waters) using an automated device in a lead-shielded hot cell. The cartridge is washed with 10.0 ml of sterile water for removing contaminants and traces of irradiated water. Finally, $^{18}$F-fluoride is eluted from the cartridge with 10.0 ml of 9 mg/ml Na Cl solution. This solution is formulated for injection using sterile filtration through sterile filter with a pore size of 0.22 µm (Millex GP, Millipore).

#### 4.3.2.2 Bone scintigraphy, SPECT, and SPECT/CT

In study II, bone scintigraphy, SPECT, and SPECT/CT imagings were performed using Symbia T6 TruePoint SPECT/CT scanner (Siemens, Erlangen, Germany). The anterior and posterior views were collected 3 hours after injection of 670 MBq $^{99m}$Tc-HDP using low-energy high-resolution (LEHR) collimators, scan speed 13 cm/min and matrix size 256x1024. Single-photon emission computed tomography combined with CT was acquired immediately after BS with following parameters: three bed positions, LEHR collimators, 90 views, 9 s scanning time per view, matrix 128x128, zoom 1.0, energy window 140 keV±15% with lower scatter window, reconstruction using Flash 3D (Siemens, Erlangen, Germany) with five iterations and ten subsets, and CT with an effective mAs 10 and 130 kVp. SPECT and SPECT/CT were performed from the top of the head to the midthighs.

#### 4.3.2.3 $^{18}$F-NaF-PET/CT

In study II, the patients were injected intravenously 209±7 (Mean, SD) MBq of $^{18}$F-NaF diluted in 3–5 ml of saline as a 60 second bolus which was quickly flushed with saline. The PET data were acquired 64±6 (mean, SD) min after the tracer injections using Discovery VCT PET/CT or PET/CT 690 scanner (General Electric Medical Systems, Milwaukee, WI, USA). A static emission scan was acquired over whole

body with three minutes (PET/CT VCT scanner) and two minutes (PET/CT 690 scanner) acquisition time per bed position. The CT scan had a noise index of 25. The sinogram data were corrected for dead time, scatter, decay, photon attenuation and reconstructed in 128x128 matrix. Image reconstruction followed a fully three-dimensional (3D) maximum likelihood ordered subsets expectation maximization algorithm incorporating CT attenuation, random and scatter corrections with 2 iterations and 28 subsets.

#### 4.3.2.4 Whole-body MRI

In study II, coronal T1-weighed (T1w), coronal short tau inversion recovery (STIR) images and DWI data were acquired using a 1.5T MR system (Avanto, Siemens, Erlangen, Germany) using surface array coils. The coronal images were collected from six table positions (table movement 250 mm) covering whole body with the following imaging parameters, T1w: repetition time/echo time (TR/TE) 709/10 ms, field of view (FOV) 500 mm, slice thickness 7.0 mm, voxel size 2.2x2.2x7.0 $mm^3$; STIR: TR/TE 14790/97 ms, inversion time 130 ms, FOV 500 mm, slice thickness 7.0 mm, voxel size 1.9x1.3x7.0 $mm^3$. The axial DWI was performed using single shot spin echo sequence with 10 table positions (table movement 100 mm), TR/TE 6300/80 ms, SPAIR fat suppression, FOV 500 mm, slice thickness 5.0 mm, voxel size 2.6x2.6x5.0 $mm^3$, three optimized diffusion directions (three-scan trace option on), b-values of 0,150,1000 $s/mm^2$. The lower limbs were covered in coronal orientation with 2–3 table positions (table movement 250 mm) and similar imaging parameters as axial DWI, except of voxel size 3.3x2.6x6.0 $mm^3$. The overall imaging time was approximately 50–60 minutes.

#### 4.3.2.5 Interpretation of nuclear images

In study II, three nuclear medicine physicians and two radiologists reviewed each imaging modality blinded from each other. The only patient information given to the interpreters was the high risk of bone metastases. Lesions were categorized as highly suspicious for being metastases, equivocal, or benign. Lesions were graded as benign on BS and SPECT scans when they were located around joints, hot osteophytes, vertically involving several ribs (indicating fracture), H-shaped pelvic abnormal, bursitis, avulsion injury, tendinitis. When the vertebral lesions involved posterior aspect, pedicle or the whole vertebral body, they were regarded as highly suspicious. Uptakes in PET/CT and SPECT images were graded as benign or highly suspicious due to corresponding morphological findings in anatomical CT images of these modalities. Typical benign lesions in CT data included bone cysts, degenerative lesions (e.g. around joints), and fractures. The tracer uptake located on osteoblastic,

osteolytic, or mixed lesions was regarded as highly suspicious based on PET/CT and/or SPECT/CT. Tracer uptakes without typical benign or malignant changes on CT were considered as equivocal.

A lesion was considered as highly suspicious on MRI if a focal or diffusion low signal intensity (SI) was present on T1w, with the corresponding intermediate or high SI on STIR and/or restricted diffusion on DWI. Typical benign lesions and/or sclerosis were interpreted according to previously published criteria (Schmidt et al., 2007; Vanel et al., 1998). Trace images (mean of 3 diffusion directions) were evaluated visually in conjunction with anatomical T1wi and STIR. No quantitative cut-off values were used for DWI.

The bone findings were compared on patient, region, and lesion level. In the region-based analysis, the skeleton was divided into five regions: head, thorax and ribs, spine, pelvis, and limbs. In the lesion-based analysis, only lesions which were highly suspicious or equivocal on at least one imaging modality were included. In addition, maximum of 5 lesions with the highest agreement between modalities per anatomical location (5 locations as defined in the region-based analysis) were included in the lesion-based analysis.

#### 4.3.2.6 Best valuable comparator (BVC)

In study II, the findings of each imaging modality were compared with best valuable comparator (BVC) in order to define their nature. Consensus reading of all imaging modalities and follow-up data of clinical, imaging, and laboratory results were used to define BVC. Highly suspicious lesions were considered as true positive if the lesions on the consensus reading of the initial imaging examinations and/or follow-up examinations were positive for bone metastases. Lesions were considered as false positive if rated as highly suspicious on one modality but as benign on consensus reading of the initial imaging examinations and/or no signs of active disease in any of the follow up examinations was discovered. False negative finding was made when a reader found no lesion or marked as a benign lesion and the consensus reading of the initial imaging examinations and/or follow-up examinations showed bone metastases. If no imaging follow-up data was available (16 PC and 12 BC patients), patients with clinical, laboratory follow-up data suggesting progression of the metastatic disease, as well as consensus reading of the initial imaging examinations suggesting metastases, were considered to have metastatic disease at the time of initial imaging (3 PC and 2 BC patients).

### 4.3.3 Methods of study III

Prostate cancer patients remitted to RT underwent MRI as a part of the planning. Thereafter, the segmentations of organs at risk and target volumes for RT were delineated manually by radiation oncologists (RO), clinical investigator (CI), and automatically by automatic segmentation tool (AST). The parameters used to compare different delineators were dice similarity coefficient values (DSC), absolute volume difference (AVD), and Hausdorff distance ($HD_{95}$), and they were calculated by the physicist. The study design of study III is shown in figure 5.

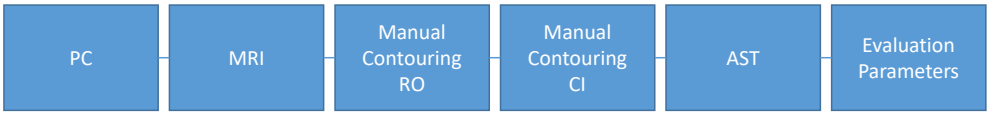


**Figure 5.** Study design of study III.

#### 4.3.3.1 Magnetic resonance imaging in radiotherapy treatment planning

In study III, all men were requested to use enema either night before or in the morning of study. They were advised to void and then drink 400 ml of water one hour before imaging which was performed with a 1.5 T MRI scanner (Philips Ingenia 1.5T HP, version 5.3.1, Philips MR Medical Systems International B.V., Best, Eindhoven, The Netherlands). This dedicated MRI RTP platform includes a flat RT-indexed couch top and an external laser positioning system (LAP GmbH Laser Applikationen, Lüneburg, Germany). In pelvic acquisition, the scanner-integrated MRI body and posterior coils were applied together with an anterior coil placed above the patient using a coil holder. The MRI scans were acquired in supine position and total imaging time was 18 minutes. No endorectal coil or gadolinium contrast was used. A second scan for those in the repeatability evaluation was obtained on the day of start of RT. The median time between the two scans was 8 (range of 6–15) days.

#### 4.3.3.2 Automated and manual segmentation of MR images

In study III, the automated segmentation tool (AST) (Philips RTdrive Core 2.0, Philips Medical Systems Netherlands B.V.) was an image post-processing tool on the Philips MRI scanner console that created standard anatomical structures required for RTP of PC parallel with the MR simulation process. The anatomical structures were generated based on MRCAT (magnetic resonance for calculating attenuation) source T1-weighted mDIXON (Dixon, 1984; Eggers et al., 2011) and T2-weighted

turbo spin echo (TSE) images. The atlas-based auto-segmentation post-processing started with 3D rigid image registration, thereby correcting for any inter-sequence motion. Subsequently, the body, prostate, seminal vesicles (SV), bladder, rectum, femoral heads, and penile bulb were segmented. To allow bladder filling and anatomic variation, the model contained typical organ shape variations.

The manual contouring process on MRI followed the ESTRO-ACROP guidelines (Salembier et al., 2018). All contouring data were divided into three groups: 1) AST, 2) the clinical investigator (CI), and 3) radiation oncologists (RO). The CI was a certified specialist in oncology (A.K.). The RO were a mixed group of specialists and residents in radiation therapy. They did the contouring as part of their routine duties. Delineations were created with an RTP system (Eclipse™ version 13.6.23, Varian Medical Systems Finland Oy, Helsinki, Finland).

Manual contouring was considered the reference method and always applied in clinical practice. AST contours were generated after all standard manual delineations had been finished, and the auto-generated contours were not used prospectively in RTP of patients. The CI was blinded to the structures contoured by the RO and vice versa. Furthermore, a radiotherapist visually inspected the AST contours for outliers, i.e. cases where the AST clearly misperformed.

#### 4.3.3.3 Geometrical parameters for evaluation

In study III, structure sets containing the contoured volumes of prostate, SV, bladder, rectum and penile bulb delineated by the CI and RO and calculated by the AST were analysed in Eclipse™ workstation. Contours manually delineated by the CI were used as ground truth. Different metrics were determined to quantify the similarity between the auto-segmented and the manually delineated volumes (Dowling et al., 2012; Guerreiro et al., 2017; Schulz et al., 2014). The formulas are represented in the original publication.

### 4.3.4 Methods of study IV

$^{11}$C-acetate-PET/CT was performed for PC patients as a planning imaging before definitive dose-escalated radiotherapy. The late toxicity was assessed on a five-year follow-up (FU) visit by the clinical oncologist (A.K). The study design of study IV is shown in Figure 6.

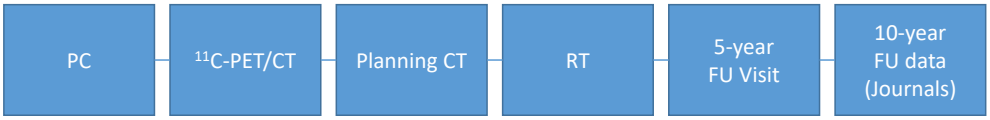


**Figure 6.** Study design of study IV.

#### 4.3.4.1 Synthesis of carbon11-acetate

An automated synthesis apparatus was used for the production of $^{11}$C-acetate from $^{11}$C-carbon dioxide. $^{11}$C-acetate was synthetized by reacting methylmagnesium bromide with $^{11}$C-carbon dioxide. The purification was performed using solvent extraction (Pike et al., 1982). The radiochemical yield of $^{11}$C-acetate was approximately 4.7 GBq for synthesis and the radiochemical purity was >99% (Seppälä et al., 2009a).

#### 4.3.4.2 $^{11}$C-acetate PET/CT

In study IV, patients were imaged with PET/CT in treatment position (flat tabletop, supine, knee support) following a 6 h fast and standard bowel preparation procedure used in the Department of Radiotherapy and Oncology of Turku University hospital, Finland. Imaging device was a combined PET/CT-scanner with 64-slice CT acquisition properties (DiscoveryTM VCE; General Electric Medical Systems, Milwaukee, WI). The PET scanner consisted of 24 rings of bismuth germanate detectors yielding 47 transverse slices spaced axially by 3.27 mm. Planning CT (120 kV, 80–440 mAs) was also used for transmission correction and had a slice thickness of 2.5 mm. The patients were requested to void 2 h before start of imaging and then drink 4–5 dl of water to maintain a standardized bladder volume during the study. A 60 s bolus of $^{11}$C-acetate diluted in 3–5 ml of saline was injected in cubital vein and promptly flushed with saline. A static 240 s emission scan was acquired 10 min after the tracer injection over the pelvic area followed by 4–5 bed positions covering the torso. The sinogram data were corrected for dead time, decay, and photon attenuation and reconstructed in a 256 x 256 matrix. Image reconstruction followed a fully 3D maximum likelihood ordered subsets expectation maximum (MLOSEM) algorithm incorporating random and scatter correction with two iterations and 28 subsets. The final in-plane FWHM (full-width half-maximum) of the system was about 6 mm. Standardized uptake value (SUV) is a widely used PET quantifier. SUVs of the ACE were calculated according to the following formula: SUV = [tissue radioactivity concentration (Bq/ml) x body weight (g)]/injected dose (Bq).

#### 4.3.4.3 RT delivery and plan evaluation in PET/CT based prostate RT

In study IV, patients underwent pre-treatment PET/CT of the pelvic region and received an intravenous mean dose of 670 MBq of $^{11}$C-acetate before start of acquisition. Based on the standardized uptake values (SUVs), metabolic target volumes (MTV) corresponding to intraprostatic lesions (IPLs) were delineated by using a median SUV 2.9 as a threshold (range 1.9 – 4.1). Two main dose levels were applied: $PTV_{low\ risk}$ and $PTV_{high\ risk}$. The $PTV_{high\ risk}$ was defined by adding a patient

anatomy-dependent 0–6 mm margin to the MTV to limit the overlap with organs at risk (OARs). Correspondingly the $PTV_{low\ risk}$ was created by expanding the prostate with an 8–10 mm margin as seen on the CT, where the smaller margin was applied to spare the rectum whenever necessary. Attention was paid to include the bases of vesicles in the $PTV_{low\ risk}$ and pelvic nodes were excluded from treatment volume in each case. Boolean operators were applied such that $PTV_{low\ risk}$ excluded $PTV_{high\ risk.}$ PET/CT applied for RT planning has been previously described in detail by Seppälä & al (Seppälä et al., 2009).

#### 4.3.4.4 Clinical follow-up

In study IV, serum PSA was measured, and the patients were seen by the treating oncologist at baseline, 3 and 12 months after the end of RT and thereafter yearly. Early toxicity was evaluated on follow-up visits 3 and 12 months after RT according to local clinical protocol. The late toxicity was evaluated on the 5-year visit by the clinical oncologist (A.K.) by international prostate symptom score (IPSS) questionnaire (Barry et al., 1992) using standard Radiation Therapy Oncology Group (RTOG) criteria taking into account medical records, physical examination and patient reported symptoms. Biochemical failure was defined by the Phoenix consensus definition as the nadir PSA concentration plus 2 ng/mL (Amling et al., 2001).

## 4.4 Statistical analysis

A $p<0.05$ was considered statistically significant in all the four studies. Statistical analyses were performed using MATLAB (Mathworks Inc., Natick, MA, USA) and/or GraphPad Software, San Diego, CA, USA) in studies I and II, and SAS System version 9.4 for Windows (SAS Institute Inc., Cary, NC) in studies III and IV.

In study I, normally distributed continuous variables were given as means and standard deviations, variables not following the normality as medians and interquartile ranges, and categorical variables as frequencies and proportions. The Kolmogorov-Smirnov test was used to check normality. ANOVA with the Bonferroni test or Kruskall-Walli's test with Dunn's test were used to compare parameter values for different tissue/cancer types, when appropriate. Two-sided p values were calculated. Diagnostic accuracy values [sensitivity, specificity, accuracy, area under the curve (AUC)] on the region level (n=12) were calculated. Sensitivity and specificity values were compared using the McNemar's test (Trajman & Luiz, 2008), and two-sided p values were calculated. Receiver operating characteristic curve (ROC) analysis using 100,000 bootstrap samples, accounting for

within-patient correlations, was used to estimate AUC values, which were compared as previously described (Hanley & McNeil, 1983); 95% confidence intervals (CIs) for AUC values also were calculated using 100,000 bootstrap samples.

In study II, equivocal findings of the imaging modalities were classified either as suggestive for metastases ("pessimistic analysis") or suggestive for non-metastatic origin ("optimistic analysis"). Sensitivity and specificity values of the patient-, region-, and lesion-based analyses were compared using McNemar's test and two-sided p-values were calculated. In region-based analysis, diagnostic accuracy values for the detection of bone metastases [sensitivity, specificity, accuracy, and AUC] were calculated from all ROIs, which were pooled into one group. Moreover, ROC analysis was performed using 60,000 bootstraps (Rutter, 2000) to account for within-patient correlations. AUC values were calculated using the trapezoid rule and compared using a method described by Hanley and McNeil (Hanley & McNeil, 1983), two-sided p-values were calculated. Bootstrap samples were constructed by stratifying patients based on overall cancer level (PC/BC present or not) and drawing patients as the independent units with replacement from these groups (PC/BC present or not) (Rutter, 2000).

In study III, all data are presented as mean with standard deviation (SD) and range, or counts and percentages. Geometrical parameters were analysed with multiway analysis of covariance (ANCOVA), including observer (AST, CI or RO) and hormones as categorical factors and body mass index (BMI) as a continuous covariate. Only if the main effect was significant (e.g. an observer) were pairwise comparisons applied. Normal distributions of the variables were evaluated from studentized residuals. Natural logarithm transformation was performed to the volumes to achieve normality of distributions. Pearson correlation coefficients were calculated for BMI and DSC difference of SV. All tests were performed as two-sided with a significance level set at 0.05. Confidence intervals of 95% for means were calculated.

Numerous sophisticated measurements and methods were used simultaneously to assess the clinical material, including patients and imaging data. This describes the multidisciplinary character of the patient management in contemporary studies.

# 5 Results

The results of each study are presented in the following. In study I (FLUCIPRO), the main aim was to discover and characterize the primary tumors and pelvic lymph nodes in the PC patients by $^{18}$F-FACBC PET/ CT, PET/MRI, and mpMRI. In study II, (SKELETA), the aim was to compare $^{99m}$Tc-HDP BS, $^{99}$Tc-HDP SPECT, $^{99m}$Tc-HPD SPECT/CT, $^{18}$F-NaF PET/CT, and whole-body 1.5T MRI, including DWI, in the accuracy of diagnosing bone metastases in high-risk PC and BC patients. In study III (AUTOCONTOURING), the main aims were to compare, evaluate and validate the delineation of organs at risk between manual and automatic tool in radiotherapy planning of PC. In study IV (ACEPRO), we aimed to evaluate the late toxicity of biology-guided dose-escalated radiotherapy in patients with prostate cancer.

## 5.1 $^{18}$F-FACBC PET/CT, PET/MRI, and mpMRI indiscovering and characterization of the primary tumors and pelvic lymph nodes in the prostate cancer patients (Study I, FLUCIPRO)

In study I, twenty-six PC patients underwent $^{18}$F-FACBC PET/CT for primary staging followed by PET/MRI with a median time of 54 (range 32–82) minutes between tracer injection and mid-frame time of PET/MRI. All patients tolerated the imaging procedure well and no adverse events were related with $^{18}$F-FACBC injections.

Robot-assisted radical prostatectomy was performed within a median of 11 (range 0–27) days after the combined PET studies; clinical and surgical findings are summarized in Table 4. Based on histopathological analysis of whole-mount prostatectomy samples, 51 tumor foci were detected in 26 patients, 41 (80%) were >0.5 cm, of which 8, 13, and 20 represented GS 3+3, 3+4, and >3+4, respectively. Positive surgical margins were identified in 8 (8/26, 30%) and seminal vesicle invasion in 9 (9/26, 35%) patients, respectively. At lymphadenectomy, a median of 16 (range 8–36; total 446) nodes were removed; metastatic involvement was found in 23 nodes of 7 (27%) patients. Residual cancer based on PSA >0.2 ng/ml at 3 months after prostatectomy was seen in two patients; original imaging for one of these patients was already suspicious for metastatic disease (Figure 7).

**Table 4.** Patient characteristics of patients in study I (FLUCIPRO). Table modified from the original publication.

| PAT. NO. | PSA [NG/ML] | GS AT BIOPSY | FLUC. TNM STAGE | FLUC. RISK GROUP | POSTOP TNM STAGE | POSTOP RISK GROUP | PET+ LN SIZE [MM] | 3 MO PSA [NG/ML] |
|---|---|---|---|---|---|---|---|---|
| **1** | 4.3 | 4+3 | T2cN0 | 3 | T2cN0 | 3 | NA | 0.003 |
| **2** | 4.1 | 4+3 | T2aN0 | 3 | T3aN0 | 3 | NA | 0.007 |
| **3** | 4.6 | 3+4 | T2cN0 | 3 | T3aN0 | 3 | NA | 0.003 |
| **4** | 8.1 | 4+3 | T2cN0 | 3 | T3aN0 | 3 | NA | 0.14 |
| **5** | 8.9 | 4+5 | T3aN0 | 3 | T3bN1 | 4 | 5 | 0.27 |
| **6** | 7.2 | 3+4 | T2aN0 | 2 | T2aN0 | 2 | NA | 0.003 |
| **7** | 7.6 | 4+3 | T3aN0 | 3 | T3aN0 | 3 | NA | 0.019 |
| **8** | 12 | 4+5 | T2cN0 | 3 | T2aN0 | 3 | NA | 0.091 |
| **9** | 8.3 | 4+3 | T2cN0 | 3 | T3aN0 | 3 | NA | 0.003 |
| **10** | 35 | 3+4 | T3bN0 | 4 | T3aN0 | 3 | NA | 0.024 |
| **11** | 6.2 | 4+3 | T2cN0 | 3 | T2cN0 | 3 | NA | 0.003 |
| **12** | 24 | 4+3 | T3bN0 | 4 | T3bN0 | 4 | NA | 0.005 |
| **13** | 16 | 4+5 | T3bN0 | 4 | T3bN0 | 4 | NA | 0.003 |
| **14** | 11 | 4+4 | T2cN0 | 3 | T3bN1 | 4 | 4.5 | 0.037 |
| **15** | 16 | 3+4 | T2cN0 | 3 | T3bN1 | 4 | 2 - 7 | 0.033 |
| **16** | 6.5 | 4+3 | T2bN0 | 3 | T3bN0 | 4 | NA | 0.005 |
| **17** | 7.7 | 3+4 | T2cN0 | 3 | T3aN0 | 3 | NA | 0.05 |
| **18** | 13 | 3+4 | T2cN0 | 3 | T3aN0 | 3 | NA | 0.003 |
| **19** | 18 | 3+4 | T2aN0 | 3 | T3aN1 | 4 | 1 | 0.003 |
| **20** | 26 | 5+4 | T3bN1M1 | 4 | T3bN1M1 | 4 | 1–25 | 5.4 |
| **21** | 5.3 | 3+4 | T2cN0 | 3 | T3aN0 | 3 | NA | 0.003 |
| **22** | 7.6 | 5+3 | T3aN0 | 3 | T3bN1 | 4 | 2 | 0.032 |
| **23** | 21 | 3+3 | T2cN0 | 3 | T2cN0 | 3 | NA | 0.003 |
| **24** | 14 | 4+5 | T3bN0 | 4 | T3bN0 | 4 | NA | 0.003 |
| **25** | 6.7 | 4+5 | T3aN0 | 3 | T3bN1 | 4 | 1.5–4.5 | 0.1 |
| **26** | 14.7 | 3+4 | T3aN0 | 3 | T2aN0 | 3 | NA | 0.026 |

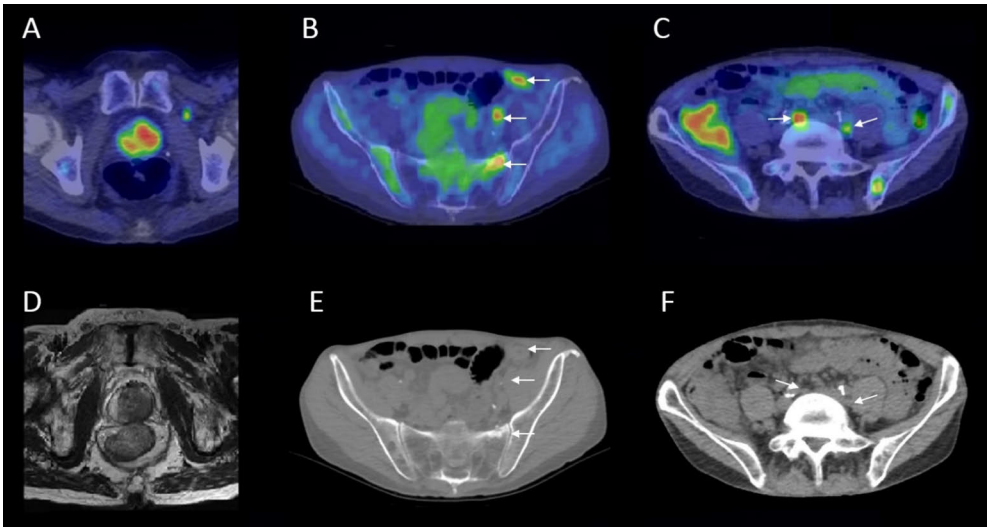


**Figure 7.** Patient who presented with PSA 26 µg/l and GS 5+4 PC on biopsy, showed uptake of $^{18}$F-FACBC in the majority of the left peripheral lobe extending from the apex to the base and to the right lobe (A). $^{18}$F-FACBC-avid metastases (white arrows) where found in left sacrum and iliac (B) and presacral lymph nodes (C). Corresponding anatomy is shown in T2w MRI (D) and CT (E, F). Figure from the original publication.

### 5.1.1 Diagnostic accuracy in region-based analysis of prostate

In the region-based analysis, 164/312 (53%) regions contained PC based on the whole-mount prostatectomy sections. Among the three modalities studied, $^{18}$F-FACBC PET/CT demonstrated the highest sensitivity (87%) and lowest specificity (56%; p<0.001), with AUC=0.72 (95%, CI 0.65.0.80; p<0.001). Sensitivity and specificity were 84% and 96% for PET/MRI and 77% (p<0.01) and 99% for mpMRI, respectively, with AUC values of 0.90 (0.86–0.94) and 0.88 (0.83–0.93), respectively. P-values are two-sided and compared to the highest values for each measure (Table 5).

**Table 5.** Diagnostic accuracy at the region level. Sensitivity, specificity and accuracy values are displayed in %. Two-sided p-values are displayed with reference to the combination marked by (*). AUC = area under the receiver operator curve; CI = confidence interval. Table 2 from the original study I.

| | SENSITIVITY | SPECIFICITY | ACCURACY | AUC (95% CI) |
|---|---|---|---|---|
| **PET/CT** | 87 (*) | 56 (p<0.001) | 72 | 0.72 (0.65-0.80) (p<0.001) |
| **PET/MRI** | 84 (p=0.32) | 96 p=0.10 | 90 | 0.90 (0.86-0.94) (*) |
| **MPMRI** | 77 (p<0.001) | 99 (*) | 88 | 0.88 (0.83-0.93) (p=0.47) |

Characteristically, index lesions were well illustrated on $^{18}$F-FACBC PET/CT and other modalities (Figure 8). $^{18}$F-FACBC PET/MRI led to significantly ($p<0.001$) improved specificity of 96% by planely reducing false-positive findings associated with tracer uptake in BPH. Both $^{18}$F-FACBC PET/MRI and mpMRI outperformed $^{18}$F-FACBC PET/CT ($p<0.01$) in AUC analysis. Diagnostic accuracy did not differ between $^{18}$F-FACBC PET/MRI and mpMRI. All identified lesions on mpMRI were scored as 5 (highly suspicious; Likert) or 4–5 (PI-RADs version 2.0) (Weinreb et al. 2016).

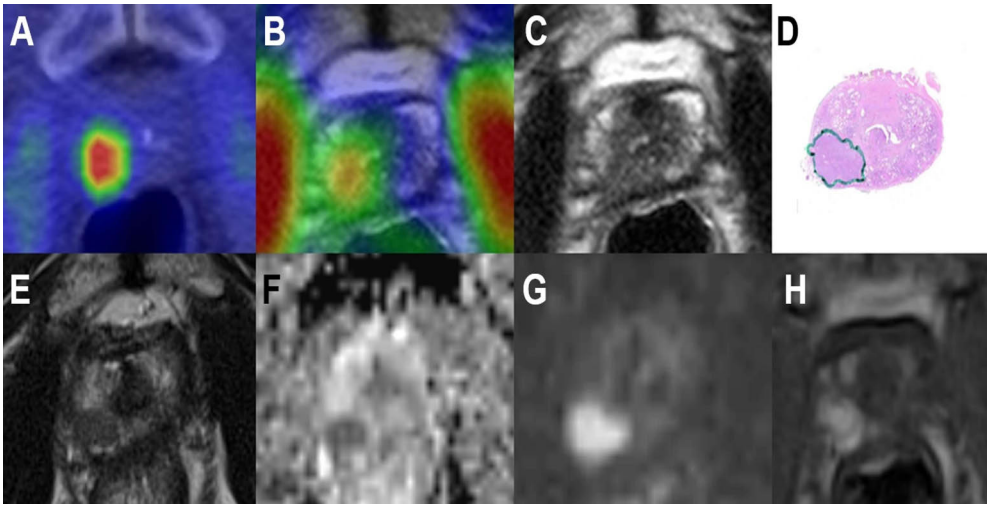


**Figure 8.** Right peripheral lesion on 18F-FACBC PET/CT (A) and PET/MRI (B); less conspicuous on T2w PET/MRI (C). Whole-mount prostatectomy section (D): tumor classified as pT3a GS 4+5. On T2w (E), ADC (F), DWI (b value=2000 s/mm2) (G), and DCE (H) of mpMRI; the lesion is well demonstrated. Note declined 18F-FACBC uptake over time for PET/CT vs PET/MRI. Figure 2 from the original publication I.

### 5.1.2 Staging accuracy (TNM)

Exact agreement between preoperative stage based on all three imaging modalities and pathological stage was seen in 12 (46%) patients. In general, no differences were detected between mpMRI and the MRI contribution of PET/MRI for T stage prediction; imaging correctly predicted stage for less than half of the cases. In 11 (42%) patients, focal 1–2 mm extra-capsular extension (stage T3a) was not identified. In 3/9 (33%) patients, seminal vesicle invasion (stage T3b) was correctly detected; a suspicion of invasion was present in two other patients on PET/MRI and mpMRI, but the related prostatectomy specimens were not positive for invasion.

Sensitivity was poor for discovering of pelvic lymph node metastases for both $^{18}$F-FACBC PET/CT and PET/MR. Hybrid PET modalities identified histologically

confirmed lymph node metastases in only 1/7 patients (17%). This patient (No. 20) had 13/22 metastatic lymph nodes and showed PET-positive left upper ramus and sacral metastases not visible on CT or scintigraphy. The size of metastatic lymph nodes not identified in the remaining six patients was less than 8 mm.

### 5.1.3 Quantitative analysis of $^{18}$F-FACBC PET/CT

Median time activity curves (Figure 4 in the original publication I) indicate early uptake of tracer in PC tumor and BPH and gradual washout that degraded the specific signal towards the end of the acquisition time. As tumor-BPH and tumor-normal prostate ratios showed, however, early imaging did not assist in discriminating cancer from BPH based on metabolic activity. The median $SUV_{max}$ of 41 cancerous lesions at 12–22 min was 4.3 (range 1.1–16.2) while it was 3.2 (range 1.3–4.2) in 22 BPH nodules and 2.9 (range 1.1–3.9) in normal prostate. Nevertheless, the SUV difference between cancer (n=41) and normal prostate (n=22) was significant ($p<0.001$), as was that between cancer and BPH ($p<0.05$) (Figure 5 in original publication I). Largely because of the higher $SUV_{max}$ of GS >3+4 compared to GS 3+4 and 3+3 tumors ($p < 0.05$), when $SUV_{max}$ values of GS 3+4 and 3+3 only were compared to BPH, differences were not significant.

The late acquisition of PET/MRI at a median of 54 (range 32–82) minutes after injection clearly reduced the specific signal compared to BPH or normal prostate. The median $SUV_{max}$ of 2.1 (range 0.8–5.5) for 41 tumors on PET/MRI did not differ significantly from that for BPH (1.7; range 0.63–2.1) or normal prostate (1.6; range 0.58–2.1).

Quantitative $^{18}$F-FACBC imaging significantly correlated with GS but did not outperform MRI in lesion recognition.

## 5.2 Comparison of the $^{99m}$Tc-HDP BS, $^{99m}$Tc-HDP SPECT, $^{99m}$Tc-HDP SPECT/CT, $^{18}$F-NaF PET/CT, and whole body 1.5 Tesla (T) MRI, including DWI (wbMRI/DWI) in the accuracy of diagnosing bone metastases in high-risk prostate cancer and breast cancer patients (study II, SKELETA)

### 5.2.1 Patient-based analysis

In study II (SKELETA), 26 BC and 27 PC patients at high risk of bone metastases underwent $^{99m}$Tc-HDP BS, $^{99m}$Tc-HDP SPECT, $^{99m}$Tc-HDP SPECT/CT, $^{18}$F-NaF PET/CT and wbMRI+DWI. The mean ± standard deviation follow-up time of 53

enrolled patients was 15±7 months while the range was 6-32 months. In total, 74 follow-up imaging examinations were performed consisting of 21 $^{99m}$Tc-HDP BS, one $^{99m}$Tc-HDP SPECT/CT, 38 CT, four $^{18}$F-NaF PET/CT, three $^{18}$F-NaF PET/MRI, and seven MRI examinations. Two PC and three BC patients died during the follow-up period. Imaging follow-up data were available for 11 PC and 14 BC patients. These studies were mainly performed in the patients with disconcordant findings among the different imaging modalities while no follow-up imaging was done in 10 PC and 10 BC patients with no highly suspicious lesion on any of the imaging modalities. These patients did not show any signs of progression during the follow-up period and were considered as true negative. Three PC patients had no imaging follow-up examinations while having highly suspicious lesion(s) on BS and/or SPECT, which were considered as false positive based on the consensus imaging findings of the initial imaging examinations.

In patient-based analysis of study II, 19 (36%, 19/53) patients, eight (30%, 8/27) PC and 11 (42%, 11/26) BC patients had presence of bone metastases based on BVC. BS had significantly lower sensitive and AUC values than $^{99m}$Tc-HDP SPECT/CT, $^{18}$F-NaF PET/CT and wbMRI+DWI (Table 6) and Figures 1 and 2 in the the original publication. When equivocal lesions were considered as suggestive for bone metastases (pessimistic analysis), $^{99m}$Tc-HDP BS and $^{99m}$Tc-HDP SPECT had significantly lower specificity values than $^{99m}$Tc-HDP SPECT/CT, $^{18}$F-NaF PET/CT, and wbMRI+DWI. Differences in sensitivity, specificity, AUC values of $^{99}$mTc-HDP SPECT/CT, $^{18}$F-NaF PET/CT, and wbMRI+DWI did not reach statistical significance.

**Table 6.** Patient-based analysis. Sensitivity, specificity, and accuracy values are displayed in %. In each group, two-sided p-values are displayed with reference to the modality marked by (*). BS; $^{99m}$Tc-hydroxymethane diphosphonate bone scintigraphy; NA: not applicable; PET/CT: $^{18}$F-NaF positron emission tomography combined with computed tomography; SPECT: $^{99m}$Tc-hydroxymethane diphosphonate single photon emission computed tomography; SPECT/CT: $^{99m}$Tc-hydroxymethane diphosphonate single photon emission computed tomography combined with computed tomography; wbMRI+DWI: whole-body MRI (T1 weighted imaging, STIR) including diffusion weighted imaging. Table from the original publication II.

| | | **OPTIMISTIC** | **ANALYSIS** | | | **PESSIMISTIC** | **ANALYSIS** | |
|---|---|---|---|---|---|---|---|---|
| | Sensitivity | Specificity | Accuracy | AUC | Sensitivity | Specificity | Accuracy | AUC |
| **BS** | 79 (p<0.001) | 91 (p<0.16) | 87 | 0.85 (p<0.05) | 85 (p<0.08) | 59 (p<0.01) | 67 | 0.72 (p<0.01) |
| **SPECT** | 89 (p=0.16) | 80 (p<0.01) | 83 | 0.84 (p<0.01) | 95 (p<0.32) | 56 (p<0.01) | 69 | 0.75 (p<0.01) |
| **SPECT/CT** | 89 (p=0.16) | 94 (p=0.32) | 93 | 0.92 (p=0.12) | 95 (p<0.32) | 88 (NA) | 90 | 0.92 (p=0.12) |
| **PET/CT** | 95 (p=0.32) | 96 (NA) | 96 | 0.96 (p=0.42) | 100 (NA) | 82 (p=0.32) | 89 | 0.91 (p=0.15) |
| **WBMRI+DWI** | 100 (*) | 97 (*) | 98 | 0.99 (*) | 100 (*) | 88 (*) | 93 | 0.94 (*) |

### 5.2.2 Region-based analysis

In region-based analysis, 58 (22%, 58/265) ROIs, 19 (14%, 19/135) PC, and 39 (30%, 39/130) BC ROIs had presence of bone metastases based on BVC (Table 7). $^{99m}$Tc-HDP BS and $^{99m}$Tc-HDP SPECT had significantly lower sensitive and AUC values than $^{99m}$Tc-HDP SPECT/CT, $^{18}$F-NaF PET/CT, and wbMRI+DWI in both pessimistic and optimistic analysis (Table 7). In pessimistic analysis, $^{18}$F-NaF PET/CT and wbMRI+DWI were significantly more sensitive than $^{99m}$Tc-HDP SPECT/CT while differences in specificity and AUC values did not reach the level of statistical significance. In contrast, when equivocal lesions were considered as not suggestive for bone metastases (optimistic analysis), the differences in sensitivity, specificity, and AUC values of $^{99m}$Tc-HDP SPECT/CT, $^{18}$F-NaF PET/CT, and wbMRI+DWI did not reach statistical significance.

**Table 7.** Region-based analysis. Sensitivity, specificity, and accuracy values are displayed in %. In each group, two-sided p-values are displayed with reference to the modality marked by (*). BS: $^{99m}$Tc-HDP bone scintigraphy; NA: not applicable; PET/CT: $^{18}$F-NaF positron emission tomography combined with computed tomography; SPECT: $^{99m}$Tc-HDP single photon emission computed tomography; SPECT/CT: $^{99m}$Tc-HDP single photon emission computed tomography combined with computed tomography; wbMRI+DWI: whole-body MRI (T1 weighted imaging, STIR) including diffusion-weighted imaging. Table from the original publication II.

| | | **OPTIMISTIC** | **ANALYSIS** | | | **PESSIMISTIC** | **ANALYSIS** | |
|---|---|---|---|---|---|---|---|---|
| | Sensitivity | Specificity | Accuracy | AUC | Sensitivity | Specificity | Accuracy | AUC |
| **BS** | 62 (p<0.001) | 98 (p=0.32) | 90 | 0.80 (p<0.001) | 72 (p<0.01) | 89 (p<0.01) | 86 | 0.81 (p<0.001) |
| **SPECT** | 74 (p<0.01) | 94 (p<0.01) | 89 | 0.83 (p<0.01) | 86 (p<0.05) | 87 (p<0.001) | 87 | 0.87 (p<0.01) |
| **SPECT/CT** | 85 (p<0.05) | 99 (p=0.32) | 96 | 0.92 (p=0.24) | 85 (p<0.01) | 98 (NA) | 90 | 0.91 (p=0.07) |
| **PET/CT** | 93 (*) | 99(*) | 98 | 0.96 (*) | 97 (*) | 97 (p=0.52) | 97 | 0.97 (*) |
| **WBMRI+DWI** | 91 (p=0.65) | 99 (p=0.32) | 97 | 0.95 (p=0.92) | 91 (p=0.25) | 98 (*) | 96 | 0.95 (p=0.36) |

### 5.2.3 Lesion-based analysis

In total, 234 lesions, 62 in PC and 172 in BC patients, were highly suspicious or equivocal in at least one imaging modality, and no more than five lesions per region with the highest agreement between modalities, as defined in the region-based analysis, were included. Of these 234 lesions, 159 (68%, 159/234) lesions, 36 (58%, 36/62) in PC and 123 (72%, 123/172) in BC patients, were considered to be metastatic bone lesions based on BVC. $^{18}$F-NaF PET/CT and wbMRI+DWI were significantly more sensitive in the lesion-based analysis than $^{99m}$Tc-HDP BS, $^{99m}$Tc-HDP SPECT, and $^{99m}$Tc-HDP SPECT/CT (Table 8). Moreover, $^{18}$F-NaF PET/CT and wbMRI+DWI had significantly higher specificity values than $^{99m}$Tc-HDP BS

and $^{99m}$Tc-HDP SPECT. $^{18}$F-NaF PET/CT and wbMRI+DWI had similar sensitivity, specificity, accuracy, and AUC values.

**Table 8.** Lesion-based analysis. Sensitivity, specificity, and accuracy values are displayed in %. In each group, two-sided p-values are displayed with reference to the modality marked by (*). BS: $^{99m}$Tc-HDP bone scintigraphy; NA: not applicable; PET/CT: $^{18}$F-NaF positron emission tomography combined with computed tomography; SPECT: $^{99m}$Tc-HDP single photon emission computed tomography; SPECT/CT: $^{99m}$Tc-HDP single photon emission computed tomography combined with computed tomography; wbMRI+DWI, whole-body MRI (T1 weighted imaging, STIR) including diffusion-weighted imaging. Table from the original publication II.

| | | **OPTIMISTIC** | **ANALYSIS** | | | **PESSIMISTIC** | **ANALYSIS** | |
|---|---|---|---|---|---|---|---|---|
| | Sensitivity | Specificity | Accuracy | AUC | Sensitivity | Specificity | Accuracy | AUC |
| **BS** | 54 (p<0.001) | 88 (p<0.01) | 65 | 0.71 (p<0.001) | 69 (p<0.001) | 72 (p<0.001) | 71 | 0.71 (p<0.001) |
| **SPECT** | 71 (p<0.001) | 79 (p<0.01) | 74 | 0.75 (p<0.001) | 77 (p<0.001) | 52 (p<0.001) | 70 | 0.65 (p<0.001) |
| **SPECT/CT** | 81 (p<0.001) | 96 (NA) | 85 | 0.88 (p=0.04) | 82 (p<0.001) | 94 (NA) | 85 | 0.88 (p=0.02) |
| **PET/CT** | 94 (p=0.78) | 96(*) | 95 | 0.95 (*) | 96 (*) | 89 (p=0.20) | 94 | 0.93 (p=0.38) |
| **WBMRI+DWI** | 95 (*) | 95 (p=0.65) | 95 | 0.95 (p=0.91) | 95 (p=0.76) | 94 (*) | 95 | 0.95 (*) |

The number of equivocal lesions was 50, 44, 5, 6, and 4 in $^{99m}$Tc-HDP BS, $^{99m}$Tc-HDP SPECT, $^{99m}$Tc-HDP SPECT/CT, $^{18}$F-NaF PET/CT, and wbMRI+DWI readings, respectively. These lesions were present in 22 (42%, 22/53), 20 (38%, 20/53), 5 (9%, 5/53), 4 (11%, 4/53), and 3 (8%, 3/53) patients of $^{99m}$Tc-HDP BS, $^{99m}$Tc-HDP SPECT, $^{99m}$Tc-HDP SPECT/CT, $^{18}$F-NaF PET/CT, and wbMRI+DWI readings, respectively. Furthermore, in 13 (25%, 13/53), 9 (17%, 9/53), 4 (8%, 4/53, 4 (8%, 4/53), and two (4%, 2/53) patients only equivocal lesions with or without benign lesions were present in $^{99m}$Tc-HDP BS, $^{99m}$Tc-HDP SPECT, $^{99m}$Tc-HDP SPECT/CT, $^{18}$F-NaF PET/CT, and wbMRI+DWI readings, respectively.

### 5.2.4 Change in patient management

In two PC patients, the detection of bone metastases discovered only by $^{99m}$Tc-HDP SPECT/CT, $^{18}$F-NaF PET/CT, and wbMRI+DWI resulted in the change of treatment (start of chemotherapy). In one BC patient, hormonal treatment was initiated due to detection of bone metastases detected by $^{18}$F-NaF PET/CT and wbMRI+DWI. Due to detection of liver and mesenteric metastases only by wbMRI+DWI, treatment plan was changed in one PC and one BC patients, respectively. These lesions were confirmed to be metastases by the imaging and clinical follow-up.

## 5.3 Evaluation and validation of an automatic segmentation tool in prostate cancer radiotherapy planning (study III, AUTOCONTOURING

A summary of results for structure volumes representing OARs is presented in Figure 9. The mean total time for contouring CTV and all OARs manually by CI was 26 (SD 7) min. Out of the 65 patients, visual inspection detected 8 prostate (12%), 4 rectum (6%), 4 bladder (6%) and 14 SV (22%) outliers in AST delineations. These were omitted from further analysis.

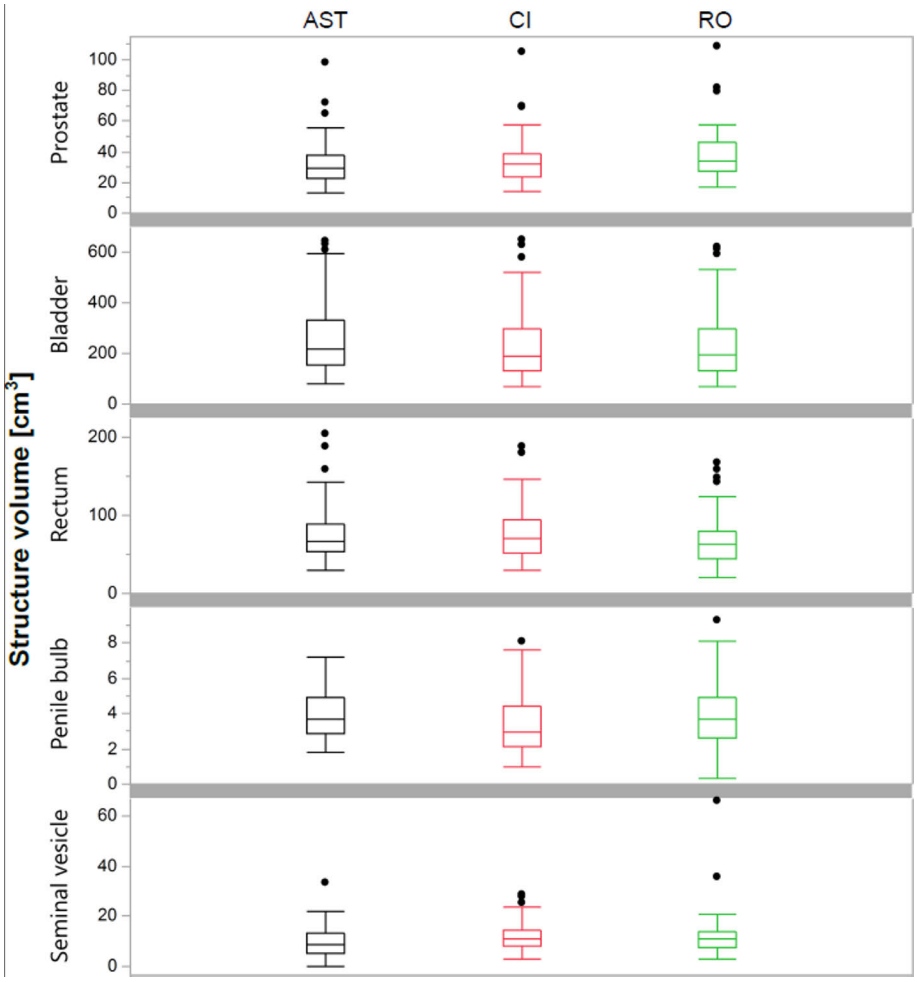


**Figure 9.** Tukey boxplots of measured structure volumes for each evaluator. AST denotes to automatic segmentation tool, CI to clinical investigator, and RO to radiation oncologist. Please note different scales for volumes on y-axes. Figure from the original publication III.

The contours of prostate, bladder, and rectum delineated manually by physicians were well comparable with those generated by the AST. The investigated geometrical parameters DSC, $HD_{95}$, and AVD between the CI or RO and the AST showed no clinically relevant differences in these structures (Figure 10). For SV and penile bulb, the concordance of manual and automated segmentation was somewhat inferior. However, this was in line with differences between the CI and RO as well.

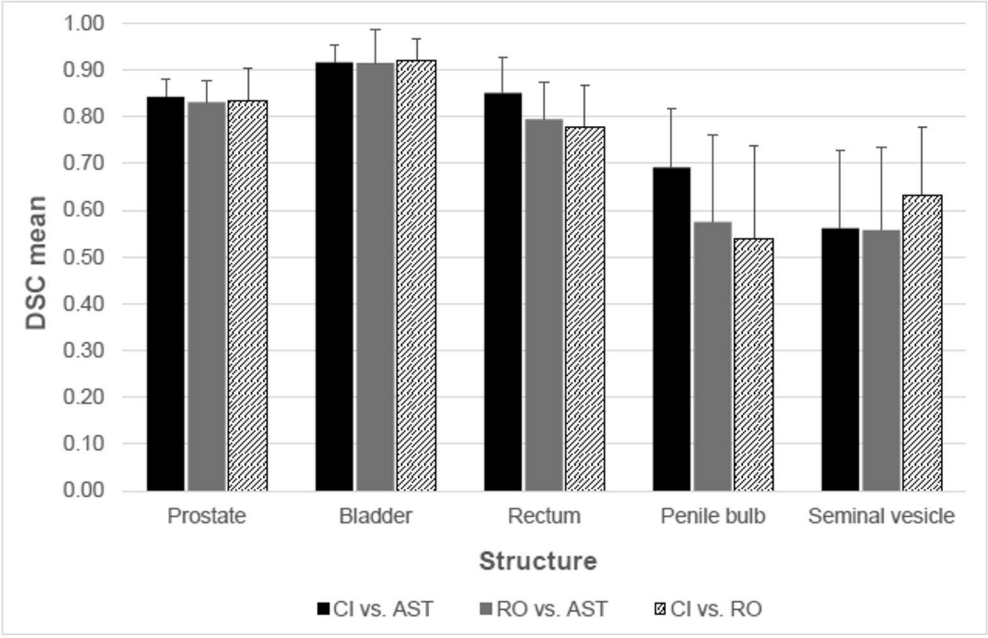


**Figure 10.** Mean dice similarity coefficient (DSC) results for contoured structures for 65 prostate cancer patients. The auto-segmented structures were compared to manually delineated structures of both radiation oncologists (RO) and clinical investigator (CI). Error bars are equal to one standard deviation. Figure from the original publication III.

Prostate, bladder and rectum centre of mass shift (CMS)s derived from CI and AST were mainly consistent within a millimetre in all coordinate directions (Figure 11). Two exceptions were revealed: the CMS in anterior-posterior (AP) direction for prostate was 1.2 mm and the CMS in head-feet (HF) direction for rectum was 1.5 mm. In further comparison of AST vs. CI, SV and penile bulb showed CMS >1 mm more frequently in AP and HF directions while the shift in LR (left-right) direction remained less than a millimetre.

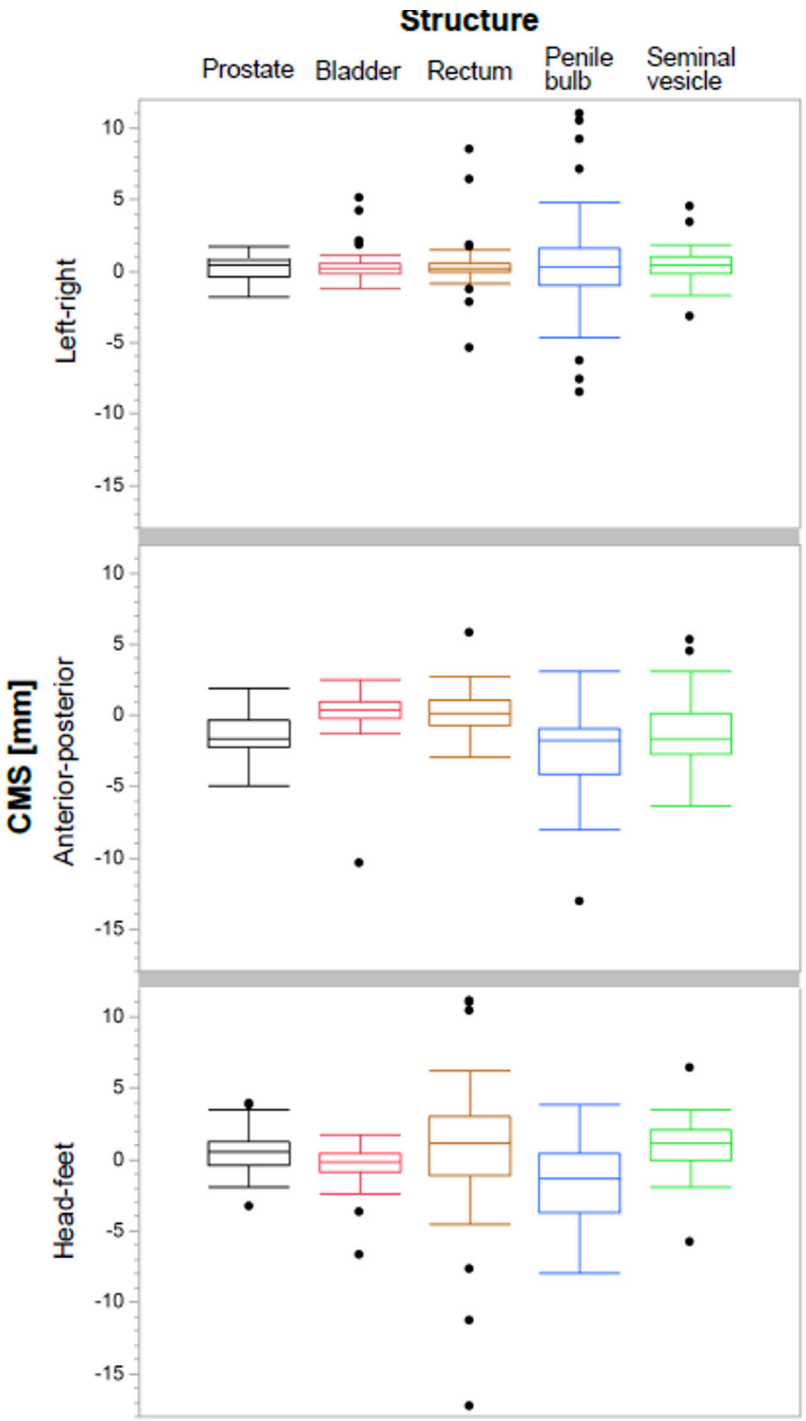


**Figure 11.** Comparison between main coordinate directions expressed as Tukey boxplots of centre of mass shift (CMS) for structures delineated by automatic segmentation tool (AST) vs. clinical investigator (CI). Figure from the original publication III.

## 5.4 The late toxicity of dose-escalated biologically guided radiotherapy in prostate cancer patients (study IV, ACEPRO)

In study IV, we followed up 30 PC patients after biologically guided dose-escalated radiotherapy treatment. Some acute but generally mild toxicity typical for contemporary RT techniques and fractionation was seen, which resolved during the first 1–2 years after RT. 5/30 (17%) patients had radiation proctitis or bleeding haemorrhoids and 2/30 (7%) patients had urinary retention or haematuria after RT. There was no grade 3 or 4 short-term toxicity.

Twenty-four out of 30 men (80%) were seen at 5-year follow-up visit for evaluation of long-term toxicity. Of these, in one patient grade 2 and in another grade 3 urinary symptoms, and in two patients grade 3 erectile symptoms were present already before RT. These patients were excluded from the toxicity evaluation. Late gastrointestinal (GI) symptoms such as diarrhoea and loose stools were uncommon. Only 1/25 patient (4%) suffered from grade 3 gastrointestinal symptoms, and no grade 2 GI symptoms were present. By contrast, erectile dysfunction was quite common, with 15/23 of men (65%) reporting Grade 2 and Grade 3 symptoms, respectively. Late GU symptoms were mostly mild, 6/23 (26%) of the patients had Grade I symptoms, and 4/23 (17%) had Grade II sympoms, respectively, while 11/23 (47%) had no GU symptoms. The toxicities at 5-year control visit are shown in Table 9.

**Table 9.** Late toxicity of 25 patients at 5-year control visit according to RTOG criteria. Number and percentage of men with given score are shown. Table from the original publication IV.

| | GRADE 0 | GRADE I | GRADE II | GRADE III | NA |
|---|---|---|---|---|---|
| **GENITOURINARY** | 11/23 (47%) | 6/23 (26%) | 4/23 (17%) | 0 | 2/23 (9%) |
| **GASTROINTESTINAL** | 21/24 (88%) | 2/24 (8%) | 0 | 1/24 (4%) | 0<br>0 |
| **ERECTILE DYSFUNCTION** | 2/23 (9%) | 4/23 (17%) | 12/23 (52%) | 3/23 (13%) | 2/23 (9%) |

# 6 Discussion

## 6.1 $^{18}$F-FACBC PET/ CT, PET/MRI, and mpMRI in discovering primary tumors and pelvic LNs in PC (Study I, FLUCIPRO)

Multimodality imaging aids in risk stratification and choice of treatment and may even predict outcome in PC (Jentsch et al., 2015). In study I, we found similar diagnostic accuracy at the regional level between $^{18}$F-FACBC PET/MRI and mpMRI, which both outperformed $^{18}$F-FACBC PET/CT in assessment of intra prostatic lesions. $^{18}$F-FACBC PET/CT demonstrated relatively low specificity of 56% because of increased tracer uptake in hyperplastic nodules, which is typical of all tracers associated with PC metabolic pathways. However, BPH could be reliably differentiated from cancer with MRI using 'high' DWI b values, clearly favoring PET/MRI over PET/CT even though PET/MRI was acquired when the $^{18}$F-FACBC tumor–prostate ratio was declining. Ideally, PET/MRI with $^{18}$F-FACBC should be perfomed no later than 10–30 min from injection, based on existing findings (Schuster et al., 2013). This time window guarantees the best lesion visibility. This is particularly essential in definitive radiotherapy including increased focal doses through SIB techniques.

$^{18}$F-FACBC has shown potential in the discovering metastatic lymph nodes among patients with biochemical recurrence after prostatectomy. This study presented the first comprehensive assessment of its potential in evaluating pelvic lymph nodes at initial staging. Only 1/7 patients, however, had $^{18}$F-FACBC-positive metastases, which measured 10–25 mm; the remaining 6 false-negative patients had metastases smaller than 8 mm. Results with DWI were comparable having low sensitivity for regional metastatic node detection.

Despite some advantages (e.g., detection of additional tumor lesions not seen on mpMRI), $^{18}$F-FACBC PET/MRI failed to outperform mpMRI in identifying intraprostatic cancer. Like previous reports, $SUV_{max}$ of BPH and tumors overlapped, emphasizing the necessity to use mpMRI with a combination of T2w and "high" b value DWI to identify hyperplastic nodules. $^{18}$F-FACBC PET/CT did demonstrate potential for predicting high-risk PCa; $SUV_{max}$ was significantly higher in tumors with GS >3+4 compared with BPH or low-GS lesions.

The most broadly used (Epstein et al., 2005) histopathological marker of prostate cancer aggressiveness is the Gleason grading system (Gleason, 1966). Development and validation of techniques facilitating non-invasive assessment of GS could improve PC risk stratification. $V_T$ derived from Logan analysis showed similar power for GS prediction as $SUV_{max}$ at 12–22 minutes, although the plots did not improve to differentiation of GSs. Dynamic PET data together with the robust measurement of $SUV_{max}$ suggest that high-risk tumors present in average with higher intracellular transport of $^{18}$F-FACBC than low-risk tumors and BPH. This may assist in image-guided biopsies and biologically guided radiotherapy.

After beginning of FLUCIPRO study, PSMA, usually labeled with $^{18}$F or $^{68}$Ga, has shown good detection rates in primary staging of PC (Hofman et al., 2020) and recurrent disease (Treglia et al., 2019) and is currently the first choice of PET tracers in PC. Because of the easy use of mpMRI in most hospitals, the role of $^{18}$F-FACBC PET as a non-invasive surrogate marker of GS is likely to be limited to academic centers. Although $^{18}$F-FACBC PET/MRI shows promise in depiction of primary prostate cancer, especially if focal ablative therapeutic approaches are planned. It is not likely, however, to replace mpMRI in routine clinical practice.

## 6.2 $^{99m}$Tc-HDP BS, $^{99m}$Tc-HDP SPECT, $^{99m}$Tc-HDP SPECT/CT, $^{18}$F-NaF PET/ CT, and (wbMRI/DWI) in diagnosing bone metastases

Accurate detection of bone metastases in PC and BC patients is essential for treatment management and patient prognosis. In study II, we assessed diagnostic accuracy of $^{99m}$Tc-MDP BS, $^{99m}$Tc-MDP SPECT, $^{99m}$Tc-MDP SPECT/CT, $^{18}$F-NaF PET/CT, and wbMRI+DWI for the discovery of bone metastases in high-risk PC and BC patients. $^{99m}$Tc-MDP SPECT/CT, $^{18F}$-NaF PET/CT and wbMRI+DWI had significantly higher AUC values for the detection of bone metastases than $^{99m}$Tc-MDP BS and $^{99m}$Tc-MDP SPECT. Furthermore, $^{18}$F-NaF PET/CT, and wbMRI+DWI showed significantly higher sensitivity and AUC values in lesion-based analysis than $^{99m}$Tc-MDP BS, $^{99m}$Tc-MDP SPECT, $^{99m}$Tc-MDP SPECT/CT (Figure 1–3 in original publication). To our knowledge, this was the first study directly comparing the diagnostic accuracy of $^{99m}$Tc-MDP BS, $^{99m}$Tc-MDP SPECT, $^{99m}$Tc-MDP SPECT/CT, $^{18}$F-NaF PET/CT, and wbMRI+DWI for the detection of bone metastases in high-risk PC and BC patients.

Our end points were purely focusing on diagnostics of bone metastases. Whole-body MRI including DWI showed high diagnostic performance for the discovering of bone metastases and was significantly more sensitive than BS, which is still the most used imaging modality for the detection of bone metastases. Large number of equivocal findings were present in BS (39%) and SPECT (38%) imaging. This often

causes repeated imaging studies, delays in diagnostics, patients' discomfort, cumulative radiation dose, and additional costs. The main difference is in the diagnostic certainty or uncertainty with BS and SPECT compared with SPECT/CT, PET/CT or wbMRI+DWI.

Our finding of wbMRI+DWI and $^{18}$F-NaF PET/CT being superior to $^{99m}$Tc-HDP BS, $^{99m}$Tc-HDP SPECT, and $^{99m}$Tc-HDP SPECT/CT for the detection of bone metastases were in line with previous results (Even-Sapir, 2005; Schirrmeister et al., 2001; Lecouvet et al., 2007). Bringing in mind the availability, cost and radiation dose, wbMRI+DWI seems to be an ideal choice in comparison with $^{18}$F-NaF PET/CT. Whole-body MRI including DWI was as accurate as $^{18}$F-NaF PET/CT for the recognition of bone metastases in our study. Furthermore, wbMRI+DWI can potentially offer valuable information regarding soft tissues and could potentially be used as a "single-step" imaging method in detecting metastases in high-risk PC, as previously suggested by Lecouvet (2012). The wide use of wbMRI+DWI for the detection of bone metastases in high-risk PC and BC patients could still be partly limited by rather long imaging time of 30-50 minutes. However, further developement of MR hardware and MR sequences could enable performing robust wbMRI+DWI in less than 30 minutes.

In this study, DWI was assessed in conjunction with T1w and STIR to diminish number of false-positive lesions (Grankvist et al., 2012), and only visual approach was used for DWI data, trace images. Quantitative evaluation of DWI could possibly allow monitoring of treatment response and early discovery of responders from those patients who need change in therapy (Messiou et al., 2011), potentially confirming a role of wbMRI+DWI as "single-step" imaging modality for detection of bone metastases in high-risk PC and BC patients.

In the current study, $^{99m}$Tc-HDP SPECT/CT, $^{18}$F-NaF PET/CT, and wbMRI+DWI were significantly more sensitive than $^{99m}$Tc-HDP BS, $^{99m}$Tc-HDP SPECT for the detection of bone metastases in high-risk PC and BC patients. Whole-body MRI, including DWI, was as accurate as $^{18}$F-NaF PET/CT for the detection of bone metastases in these high-risk patients. Whole-body MRI, including DWI, seems to be the preferred imaging modality for the detection of bone metastases in high-risk BC and PC patients in comparison with $^{99m}$Tc-HDP BS, $^{99m}$Tc-HDP SPECT, $^{99m}$Tc-HDP SPECT/CT, and $^{18}$F-NaF PET/CT. In the context of nuclear medicine techniques, $^{99m}$Tc-HDP SPECT/CT was superior to $^{99m}$Tc-HDP BS, $^{99m}$Tc-HDP SPECT, and $^{99m}$Tc-HDP SPECT/CT had less equivocal findings.

## 6.3 Performance of AST in RTP of PC (study III, AUTOCONTOURING)

Study III explored the function of AST to generate clinically relevant delineations for RTP of PC. A commercial model-based algorithm developed for MRI only and automated RTP workflow was engaged. In comparison to the manual segmentations, regarding DSC, AST presented high agreement for prostate, bladder, rectum, and moderate agreement for seminal vesicles and penile bulb. Visual assessment exposed a few obvious outliers, which would have been manually revised for in a clinical setting and were therefore excluded from the analysis. The CMS revealed a systematic 1 mm shift in the AP direction. Compared with visual inspection of the results, this difference did not seem clinically relevant. The found $HD_{95}$ values (in Supplementary Table 3 in the original publication) are in line with those reported by Delpon et al. (2016), and Wong et al. (2020), who both studied CT-based auto-segmentation tools. Specially, for the prostate the $HD_{95}$ of 4.6 mm (95% confidence interval 4.3 – 4.9 mm) is smaller to that reported by Wong (6.7 mm), indicating that MRI-based delineation may increase accuracy.

The performance of AST was nearly independent of BMI and feasible for both men on and off hormonal therapy, even if the latter group tended to smaller prostate and SV volumes. Although the difference in prostate volumes between those off and on treatment was significant ($p=0.0001$), the small number of hormone naïve patients indicates that further studies are needed to confirm our observation. However, short-term neoadjuvant hormonal therapy seems to reduce the size of prostate also in our patients in accordance with other reports (Axcrona et al., 2012).

Previously, MRI-based prostate segmentation has mainly been used for diagnostic applications, while only few studies have attempted to delineate prostate and SV for RTP. However, these studies have established small inter-physician variability (0.7–1.7 mm) (Nyholm et al., 2013) and good volume overlap (0.78–0.88) for prostate, bladder and rectum between automatic and manual contourings (Pasquier et al., 2007). In our study, good consistency between automated and manual delineation of prostate, SV, and OAR was indeed detected, and the inter-observer variability was comparable to preceding studies (Nyholm et al., 2013).

It is generally accepted that a DSC > 0.7, 0.5-0.7, or < 0.5 signifies good, moderate or poor agreement between reference and test structures, respectively (Zijdenbos et al., 1994). While our DSC metrics comparing manual and automatic segmentation resulted in good agreement for the most essential RTP organs, the findings for the seminal vesicles and penile bulb showed only moderate agreement. In general, the reliability of segmentation depends, among other things, on the volume and composition of the structures. This explains the moderate DSCs for the smaller organs e.g. SV and penile bulb, both between AST and CI as well as RO and CI. In line with this, the visualization of penile bulb is poor even by MRI and prone

to subjective concepts about its differentiation from the body of the penis. Langmack et al. (2014) found poor agreement for SV in their study with atlas-assisted segmentation based on both CT and MRI. They assumed it to be reflection of both the difficulty in visualizing them and determining which part of them to outline.

In general, there is a remarkable variability in earlier reported DSC values which reflects the numerous differences in protocols used for RTP. For instance, Dowling et al. (Dowling, et al. 2012) described DSCs denoting moderate agreement for prostate, bladder, and rectum of 0.70, 0.64, and 0.63, respectively. Korsager et al. (2015), on the other hand, reported a mean DSC of 0.88 for prostate. Delpon et al. (2016), compared delineations formed from CT images by a radiation oncologist to contours computed by five different automated atlas-based segmentation algorithms, and the mean DSC varied between 0.59 and 0.81 for the bladder and between 0.49 and 0.75 for the rectum.

## 6.4 Late toxicity in PC patients after dose-escalated RT (study IV, ACEPRO)

Study IV was designed to assess the impact of $^{11}$C-acetate PET/CT on outcome of IMRT in patients with localized PC. Our goal was to decrease toxicity by dose-escalating tumor dose by applying SIB delineated with metabolic imaging. Interest in focal approach of PC RT will soon define role of multimodality imaging with PET and MRI in SIB-IMRT and our results reported outcome of such a technique.

PET is now routinely used for diagnosis, staging, and therapy monitoring in oncology, but the general-purpose tracer $^{18}$F-fluoro-2-deoxy-D-gluocose (FDG) is, unlike its natural substrate analogue glucose, secreted in urine and shows low uptake in early PC (Machtens et al., 2007).

PET with prostate-specific membrane antigen (PSMA) ligands is now recommended for assessment of PC after biochemical recurrence (Cornford et al., 2021). Hofman et al suggested to replace conventional CT imaging and bone scan with PSMA PET imaging in high-risk PC patients in staging before curative-targeted therapy, since it is shown to reveal metastases more accurately and can be used as a single-step method (Hofman et al., 2020). Nevertheless, the use of PSMA PET/CT in staging or management of localized PC is less well established, although promising (Grubmuller et al., 2018). However, at the time of patient enrolment of our ACEPRO study, PSMA was not available. We therefore used ACE for therapy planning since it has showed minimal excretion in urine and has appeared to be feasible for evaluating patients experiencing PSA relapse after RT or radical prostatectomy (Oyama et al., 2002). Uptake of ACE in PC is based on altered lipid metabolism, and although some uptake in benign prostatic hyperplasia does occur, it does not compromise biologically modified IMRT plan if whole prostate dose is

de-escalated compared to the standard plan. In line with this, we were able to design plans with low rectum and bladder doses (Figure 3 in the original publication IV), which translated to a low toxicity at 5 years considering the modestly escalated dose in IPL(s).

Other dose painting studies have used different PET tracers and multiparametric MRI in their protocols (Monninkhof et al., 2018). Kerkmeijer et al (2021) evaluated the late toxicity two years after MRI-defined RT of 77 Gy in 35 fractions (n=287) with an MRI-defined SIB up to 95Gy (n=284). Focal dose escalation did not result in an increase in GU or GI toxicity in intermediate- or high-risk PC patients. Yu et al.,(2013) applied $^{111}$In-capromab pendetide (ProstaScint) gamma imaging for dose painting of intraprostatic lesion to 82 Gy, while the rest of prostate received 75.6 Gy. In line with our study, the incidence of long-term Grade 3-4 toxicity was low. Also, Vora et al. reported similar 5-year toxicity rates in IMRT-treated PC patients who received a mean radiation dose of 75.6 Gy (Vora et al., 2007). In comparison to these two studies our results are encouraging, in particular if higher dose escalation of 85-90 Gy (Koskela et al., 2017) would be applied to the IPLs while maintaining de-escalation of the dose in whole prostate at current level.

## 6.5 Limitations of the study

In study I (FLUCIPRO), the potential limitation is the relatively long time to PET/MRI imaging after the injection of $^{18}$F-FACBC. Shorter time window would have ensured the best lesion visibility. Also, some patients had large amount of rectal gas or mass, which could cause intestinal movement and therefore also affect the quality of imaging and reading.

The main limitation of study II (SKELETA) is the correct evaluation of true nature of the lesions since histological confirmation was not available. Clinical and imaging follow-up of at least 6 months (mean±SD, min, max: 15±7, 6, 32, months) in addition to consensus reading of all imaging modalities was used to define true nature of the lesions detected by each of the modalities. However, this approach can result in overestimation of diagnostic accuracy of the most accurate imaging modality (Lecouvet et al., 2012). Differences in experience of $^{99m}$Tc-HDP BS, $^{99m}$Tc-HDP SPECT, $^{99m}$Tc-HDP SPECT/CT, $^{18}$F-NaF PET/CT, and wbMRI+DWI interpreters could potentially have impact on the results. However, all the readers had high expertise in nuclear medicine as physicians and/or radiologists. This study is further limited by moderately small number of patients.

A potential limitation of study III (AUTOCONTOURING) is the use of only one delineator (CI) as a reference contouring physician. CI contouring was considered "the gold standard" but cannot be regarded to denote the absolute ground truth due to inter-observer variability (Balagopal et al., 2018). On the other hand, the

evaluation of DSC between CI and RO showed high agreement, demonstrating concordance between multiple delineators with varying amounts of experience. In essence, we wanted to assess the feasibility and reproducibility of AST for clinical use. Another limitation was that the investigated AST was vendor and machine dependent, which constrained its accessibility. Furthermore, for patients unsuitable for MRI or those with hip prostheses, automatic contouring was not possible.

In study IV (ACEPRO), a limitation for use of ACE in treatment planning is its potential sensitivity to androgen depletion, which decreases uptake in prostate of patients on neoadjuvant hormonal treatment. We have comprehended this phenomenon clinically and excluded therefore patients receiving hormonal therapy in the enrollment in our study. The research was further limited by relatively small number of patients, especially in the low-risk group. Another limitation was lack of baseline evaluation of urinary, GI and erectile function, which was, however, of minor importance since only one patient reported late G3 gastro-intestinal toxicity.

# 7 Conclusions

I $^{18}$F-FACBC PET/MRI shows promise in characterization of primary PC, especially if focal ablative therapeutic modalities are planned. However, mpMRI will most likely remain in routine clinical practice due to its easy use in most hospitals. The role of $^{18}$F-FACBC PET as a non-invasive surrogate marker of GS is likely to be limited to academic centers.

II $^{99m}$Tc-HDP SPECT/CT, $^{18}$F-NaF PET/CT, and wbMRI+DWI are significantly more sensitive than $^{99m}$Tc-HDP BS and $^{99m}$Tc-HDP SPECT for detection of bone metastasis in high-risk PC and BC patients. $^{18}$F-NaF PET/CT and wbMRI+DWI reaches the same level of accuracy in bone metastasis detection in these high-risk cancer patients. When comparing nuclear medicine techniques, $^{99m}$Tc-HDP SPECT/CT shows its superiority to $^{99m}$Tc-HDP BS, and SPECT by having less equivocal findings.

III Automatic segmentation tool shows good agreement and accuracy in delineating prostate, bladder, and rectum in MRI-only based radiotherapy planning of prostate cancer, when compared with manual delineations of clinicians. However, manual assessment and adjustment of some structures remain important in clinical use.

IV Biological guidance for dose-escalated whole-prostate RT is feasible with $^{11}$C-ACE PET/CT and does not seem to increase late toxicity.

In conclusion, the novel imaging modalities have enabled more accurate diagnostics, staging, and treatment of prostate cancer. Modern automatic tools provide useful help in clinical practice and are already implemented in hospital routine.

# Acknowledgements

This work was carried out at the Department of Oncology and Radiotherapy of Turku University Hospital, the Medical Imaging Center of Southwest Finland, University of Turku, and the Turku PET Centre during 2012–2022.

I would like to express my sincere gratitude to the following people who supported me during this time:

My principal supervising professor Heikki Minn, Department of Oncology and Radiotherapy, introduced me to these research projects. Professor Minn has a vast knowledge of the field of medical oncology and profound expertise in practical patient work. He is genuinely enthusiastic about the topics he is lecturing on or researching, and he inspires others with his visionary energy. His deep warmth and understanding have made him easy to approach. Despite all his important obligations, he has always been available when his assistance was needed. To him I owe my deepest gratitude.

Docent Marko Seppänen, my other supervisor with a comprehensive knowledge of nuclear medicine, supported me right from the start of the first project (SKELETA). Thesis follow-up committee member Docent Paula Lindholm for continual, positive support on my doctoral studies and in my clinical work, offering her extensive experience in radiotherapy and research. I am profoundly grateful to them both.

The reviewers of the thesis, Docents Antti Loimaala and Juha Nikkinen, offered valuable comments and remarks, greatly improving the thesis manuscript. My deepest thanks to them both.

Thank you to all the co-authors of the original publications for your great collaboration and flexibility: Ivan Jambor, MD PhD, for the enormous amount of work done analyzing the images and other data and writing the manuscripts. You have shown me how totally dedicated somebody can be to the world of science. Docent Jukka Kemppainen, for analyzing the PET/CT and PET/MR images, biostatisticians Jaakko Matomäki, Mari Koivisto, and Eliisa Löyttyniemi, MSc, for your contribution to applying statistical methods in the studies, and physicist Marko Pesola, for your validation of the autocontouring tool.

Physicists Pauliina Wright and Sami Suilamo, Iiro Ranta, Jani Keyriläinen, Jan Seppälä, and Jani Saunavaara, for your expertise in radiotherapy and medical imaging and your invaluable analysis of the data and results.

Pathologist Markku Kallajoki, for reviewing the histopathological material for the ACEPRO study, and Pekka Taimen for the FLUCIPRO study.

Psychologist Florence Schmidt, PhD, for mentoring me through both the scientific and psychological challenges, for giving wise and practical, deeply sympathetic, advice throughout my time working at this hospital.

The staff of Turku PET Centre and KLIP for your excellent collaboration and professional work.

All my colleagues and workmates at Turku University Hospital for pleasant working days and friendship, sharing the joys, frustrations, and difficulties.

I am very grateful to have so many close friends around me who have shared their lives, tears, and laughter with me. You have listened, spoken, sung, and danced with me when I needed it.

Mom, thank you for all your physical and financial support. You have always been there for me and have done everything possible (from babysitting to renovation) to help me. Dad, thank you for all the conversations and support you have given me. You have taught me how to be compassionate towards others and myself. You have shown me that the strongest people are brave enough to show their weakness. My siblings, you and your families are the joy of my everyday life. I know I am never alone because I have you. You relieve my pain with a joke but are still not afraid of my tears or serious thoughts.

To my husband's family, parents-in-law, brothers-in-law, and your families, thank you for the warm welcome to your clan—for all the support and experiences we have shared together, for your crucial help in helping take care of our daughters, and expanding our small family with so many special and caring people.

Finally, my special thanks are addressed to my family. My dear ex-husband Juha, you have worked unbelievably hard for this family. Without you, we would not have had our beautiful home and relaxing summer cottage, or the wonderful memories together. You are the most warmhearted father anyone could ask for. And you have given me the two most precious and wonderful girls in the world. Ella, your warmhearted kindness and beauty, endless playfulness and energy have given me so much. Thank you for having me in your life. Emma, you were my biggest dream, and you came true.

This study was financially supported by the National Graduate School of Clinical Investigation, State Research Funding of Turku University Hospital, Cancer Foundation Finland, Ida Montin Foundation, Turku Cancer Research Society/Cargotec, Southwest Finland Cancer Society and The Finnish Medical Foundation.

November 21th, 2022
*Anna Kuisma*

# References


Albrecht, S., Buchegger, F., Soloviev, D., Zaidi, H., Vees, H., Khan, H. G., Keller, A., Bischof Delaloye, A., Ratib, O., & Miralbell, R. (2007). (11)C-acetate PET in the early evaluation of prostate cancer recurrence. *European Journal of Nuclear Medicine and Molecular Imaging*, *34*(2), 185–196. https://doi.org/10.1007/S00259-006-0163-X

Amling, C. L., Bergstralh, E. J., Blute, M. L., Slezak, J. M., & Zincke, H. (2001). Defining prostate specific antigen progression after radical prostatectomy: what is the most appropriate cut point? *The Journal of Urology*, *165*(4), 1146–1151.

*Assessment of malignant skeletal disease: initial experience with 18F-fluoride PET/CT and comparison between 18F-fluoride PET and 18F-fluoride PET/CT - PubMed*. (n.d.). Retrieved May 29, 2022, from https://pubmed.ncbi.nlm.nih.gov/14960647/

Axcrona, K., Aaltomaa, S., da Silva, C. M., Özen, H., Damber, J.-E., Tankó, L. B., Colli, E., & Klarskov, P. (2012). Androgen deprivation therapy for volume reduction, lower urinary tract symptom relief and quality of life improvement in patients with prostate cancer: degarelix vs goserelin plus bicalutamide. *BJU International*, *110*(11), 1721–1728. https://doi.org/10.1111/j.1464-410X.2012.11107.x

Balagopal, A., Kazemifar, S., Nguyen, D., Lin, M. H., Hannan, R., Owrangi, A., & Jiang, S. (2018). Fully automated organ segmentation in male pelvic CT images. *Physics in Medicine and Biology*, *63*(24). https://doi.org/10.1088/1361-6560/AAF11C

Barry, M. J., Fowler, F. J., O'Leary, M. P., Bruskewitz, R. C., Holtgrewe, H. L., Mebust, W. K., & Cockett, A. T. (1992). The American Urological Association symptom index for benign prostatic hyperplasia. The Measurement Committee of the American Urological Association. *The Journal of Urology*, *148*(5), 1549–1557; discussion 1564.

Bell, K. J. L., del Mar, C., Wright, G., Dickinson, J., & Glasziou, P. (2015). Prevalence of incidental prostate cancer: A systematic review of autopsy studies. *International Journal of Cancer*, *137*(7), 1749–1757. https://doi.org/10.1002/ijc.29538

Bettinardi, V., Presotto, L., Rapisarda, E., Picchio, M., Gianolli, L., & Gilardi, M. C. (2011). Physical performance of the new hybrid PET/CT Discovery-690. *Medical Physics*, *38*(10), 5394–5411. https://doi.org/10.1118/1.3635220

Bomers, J. G. R., & Barentsz, J. O. (2014). Standardization of multiparametric prostate MR imaging using PI-RADS. *BioMed Research International*, *2014*. https://doi.org/10.1155/2014/431680

Brierley, J. D., Gospodarowicz, M. K., & Wittekind, C. (2016). *Publications and Resources | UICC*. The TNM Classification of Malignant Tumours 8th Edition. https://www.uicc.org/resources/tnm/publications-resources

*Cancer in Finland - Syöpärekisteri*. (n.d.). Retrieved May 29, 2022, from https://cancerregistry.fi/statistics/cancer-in-finland/

Cellini, N., Morganti, A. G., Mattiucci, G. C., Valentini, V., Leone, M., Luzi, S., Manfredi, R., Dinapoli, N., Digesu', C., & Smaniotto, D. (2002). Analysis of intraprostatic failures in patients treated with hormonal therapy and radiotherapy: implications for conformal therapy planning. *International Journal of Radiation Oncology, Biology, Physics*, *53*(3), 595–599. https://doi.org/10.1016/S0360-3016(02)02795-5

Chen, M. E., Johnston, D. A., Tang, K., Babaian, R. J., & Troncoso, P. (2000). Detailed mapping of prostate carcinoma foci. *Cancer*, *89*(8), 1800–1809. https://doi.org/10.1002/1097-0142(20001015)89:8<1800::AID-CNCR21>3.0.CO;2-D

Corfield, J., Perera, M., Bolton, D., & Lawrentschuk, N. (2018). 68 Ga-prostate specific membrane antigen (PSMA) positron emission tomography (PET) for primary staging of high-risk prostate cancer: a systematic review. *World Journal of Urology*, *36*(4), 519–527. https://doi.org/10.1007/S00345-018-2182-1

Cornford, P., van den Bergh, R. C. N., Briers, E., van den Broeck, T., Cumberbatch, M. G., de Santis, M., Fanti, S., Fossati, N., Gandaglia, G., Gillessen, S., Grivas, N., Grummet, J., Henry, A. M., der Kwast, T. H. van, Lam, T. B., Lardas, M., Liew, M., Mason, M. D., Moris, L., … Mottet, N. (2021). EAU-EANM-ESTRO-ESUR-SIOG Guidelines on Prostate Cancer. Part II—2020 Update: Treatment of Relapsing and Metastatic Prostate Cancer. *European Urology*, *79*(2), 263–282. https://doi.org/10.1016/j.eururo.2020.09.046

D'amico, A. v, Whittington, ; Richard, Malkowicz, ; S Bruce, Schultz, D., Blank, K., Broderick, G. A., Tomaszewski, J. E., Renshaw, A. A., Kaplan, I., Beard, C. J., & Wein, A. (n.d.). *Biochemical Outcome After Radical Prostatectomy, External Beam Radiation Therapy, or Interstitial Radiation Therapy for Clinically Localized Prostate Cancer*. https://jamanetwork.com/

Dasu, A., & Toma-Dasu, I. (2012). Prostate alpha/beta revisited -- an analysis of clinical results from 14 168 patients. *Acta Oncologica (Stockholm, Sweden)*, *51*(8), 963–974. https://doi.org/10.3109/0284186X.2012.719635

Delpon, G., Escande, A., Ruef, T., Darréon, J., Fontaine, J., Noblet, C., Supiot, S., Lacornerie, T., & Pasquier, D. (2016). Comparison of automated atlas-based segmentation software for postoperative prostate cancer radiotherapy. *Frontiers in Oncology*, *6*(AUG). https://doi.org/10.3389/FONC.2016.00178/ABSTRACT

DeMarzo, A. M., Nelson, W. G., Isaacs, W. B., & Epstein, J. I. (2003). Pathological and molecular aspects of prostate cancer. *Lancet (London, England)*, *361*(9361), 955–964. https://doi.org/10.1016/S0140-6736(03)12779-1

Dixon, W. T. (1984). Simple proton spectroscopic imaging. *Radiology*, *153*(1), 189–194. https://doi.org/10.1148/radiology.153.1.6089263

Dowling, J. A., Lambert, J., Parker, J., Salvado, O., Fripp, J., Capp, A., Wratten, C., Denham, J. W., & Greer, P. B. (2012). An atlas-based electron density mapping method for magnetic resonance imaging (MRI)-alone treatment planning and adaptive MRI-based prostate radiation therapy. *International Journal of Radiation Oncology, Biology, Physics*, *83*(1). https://doi.org/10.1016/J.IJROBP.2011.11.056

Drost, F.-J. H., Osses, D. F., Nieboer, D., Steyerberg, E. W., Bangma, C. H., Roobol, M. J., & Schoots, I. G. (2019). Prostate MRI, with or without MRI-targeted biopsy, and systematic biopsy for detecting prostate cancer. *Cochrane Database of Systematic Reviews*. https://doi.org/10.1002/14651858.cd012663.pub2

Eggers, H., Brendel, B., Duijndam, A., & Herigault, G. (2011). Dual-echo Dixon imaging with flexible choice of echo times. *Magnetic Resonance in Medicine*, *65*(1), 96–107. https://doi.org/10.1002/mrm.22578

Epstein, J. I. (2010). An update of the Gleason grading system. *The Journal of Urology*, *183*(2), 433–440. https://doi.org/10.1016/J.JURO.2009.10.046

Epstein, J. I., Allsbrook, W. C., Amin, M. B., Egevad, L. L., Bastacky, S., López Beltrán, A., Berner, A., Billis, A., Boccon-Gibod, L., Cheng, L., Civantos, F., Cohen, C., Cohen, M. B., Datta, M., Davis, C., Delahunt, B., Delprado, W., Eble, J. N., Foster, C. S., … Young, R. H. (2005). The 2005 International Society of Urological Pathology (ISUP) Consensus Conference on Gleason Grading of Prostatic Carcinoma. *The American Journal of Surgical Pathology*, *29*(9), 1228–1242. https://doi.org/10.1097/01.PAS.0000173646.99337.B1

Epstein, J. I., Egevad, L., Amin, M. B., Delahunt, B., Srigley, J. R., & Humphrey, P. A. (2016). The 2014 International Society of Urological Pathology (ISUP) Consensus Conference on Gleason

Grading of Prostatic Carcinoma: Definition of Grading Patterns and Proposal for a New Grading System. *The American Journal of Surgical Pathology*, *40*(2), 244–252. https://doi.org/10.1097/PAS.0000000000000530

Evans, J. D., Jethwa, K. R., Ost, P., Williams, S., Kwon, E. D., Lowe, V. J., & Davis, B. J. (2018). Prostate cancer-specific PET radiotracers: A review on the clinical utility in recurrent disease. *Practical Radiation Oncology*, *8*(1), 28–39. https://doi.org/10.1016/J.PRRO.2017.07.011

Even-Sapir E. Imaging of malignant bone involvement by morphologic, scintigraphic, and hybrid modalities. *J Nucl Med. 2005 Aug;46*(8):1356-67. PMID: 16085595.

Fossati, N., Willemse, P. P. M., van den Broeck, T., van den Bergh, R. C. N., Yuan, C. Y., Briers, E., Bellmunt, J., Bolla, M., Cornford, P., de Santis, M., MacPepple, E., Henry, A. M., Mason, M. D., Matveev, V. B., van der Poel, H. G., van der Kwast, T. H., Rouvière, O., Schoots, I. G., Wiegel, T., … Joniau, S. (2017). The Benefits and Harms of Different Extents of Lymph Node Dissection During Radical Prostatectomy for Prostate Cancer: A Systematic Review. In *European Urology* (Vol. 72, Issue 1, pp. 84–109). Elsevier B.V. https://doi.org/10.1016/j.eururo.2016.12.003

Gleason, D. F. (1966). Classification of prostatic carcinomas. *Cancer Chemotherapy Reports*, *50*(3), 125–128. https://pubmed.ncbi.nlm.nih.gov/5948714/

Grankvist, J., Fisker, R., Iyer, V., Fründ, E. T., Simonsen, C., Christensen, T., Stenbygaard, L., Ewertz, M., & Larsson, E. M. (2012). MRI and PET/CT of patients with bone metastases from breast carcinoma. *European Journal of Radiology*, *81*(1). https://doi.org/10.1016/J.EJRAD.2010.10.024

Grubmuller, B., Baltzer, P., Hartenbach, S., D'Andrea, D., Helbich, T. H., Haug, A. R., Goldner, G. M., Wadsak, W., Pfaff, S., Mitterhauser, M., Balber, T., Berroteran-Infante, N., Grahovac, M., Babich, J., Seitz, C., Kramer, G., Susani, M., Mazal, P., Kenner, L., … Hartenbach, M. (2018). PSMA Ligand PET/MRI for Primary Prostate Cancer: Staging Performance and Clinical Impact. *Clinical Cancer Research : An Official Journal of the American Association for Cancer Research*, *24*(24), 6300–6307. https://doi.org/10.1158/1078-0432.CCR-18-0768

Guerreiro, F., Burgos, N., Dunlop, A., Wong, K., Petkar, I., Nutting, C., Harrington, K., Bhide, S., Ourselin, S., Oelfke, U., & Knopf, A. C. (2017). Physica Medica Evaluation of a multi-atlas CT synthesis approach for MRI-only radiotherapy treatment planning. *Physica Medica*, *35*, 7–17. https://doi.org/10.1016/j.ejmp.2017.02.017

Hamdy, F. C., Donovan, J. L., Lane, J. A., Mason, M., Metcalfe, C., Holding, P., Davis, M., Peters, T. J., Turner, E. L., Martin, R. M., Oxley, J., Robinson, M., Staffurth, J., Walsh, E., Bollina, P., Catto, J., Doble, A., Doherty, A., Gillatt, D., … Neal, D. E. (2016). 10-Year Outcomes after Monitoring, Surgery, or Radiotherapy for Localized Prostate Cancer. *New England Journal of Medicine*, *375*(15), 1415–1424. https://doi.org/10.1056/nejmoa1606220

Hanley, J. A., & McNeil, B. J. (1983). A method of comparing the areas under receiver operating characteristic curves derived from the same cases. *Radiology*, *148*(3), 839–843. https://doi.org/10.1148/RADIOLOGY.148.3.6878708

Hayes, J. H., & Barry, M. J. (2014). Screening for prostate cancer with the prostate-specific antigen test: a review of current evidence. *JAMA*, *311*(11), 1143–1149. https://doi.org/10.1001/JAMA.2014.2085

Hemminki, K. (2012). Familial risk and familial survival in prostate cancer. *World Journal of Urology*, *30*(2), 143–148. https://doi.org/10.1007/S00345-011-0801-1

Hofman, M. S., Lawrentschuk, N., Francis, R. J., Tang, C., Vela, I., Thomas, P., Rutherford, N., Martin, J. M., Frydenberg, M., Shakher, R., Wong, L. M., Taubman, K., Ting Lee, S., Hsiao, E., Roach, P., Nottage, M., Kirkwood, I., Hayne, D., Link, E., … Murphy, D. G. (2020). Prostate-specific membrane antigen PET-CT in patients with high-risk prostate cancer before curative-intent surgery or radiotherapy (proPSMA): a prospective, randomised, multicentre study. *Lancet (London, England)*, *395*(10231), 1208–1216. https://doi.org/10.1016/S0140-6736(20)30314-7

Hövels, A. M., Heesakkers, R. A. M., Adang, E. M., Jager, G. J., Strum, S., Hoogeveen, Y. L., Severens, J. L., & Barentsz, J. O. (2008). The diagnostic accuracy of CT and MRI in the staging of pelvic

lymph nodes in patients with prostate cancer: a meta-analysis. *Clinical Radiology*, *63*(4), 387–395. https://doi.org/10.1016/j.crad.2007.05.022

Huang, C., & Mcconathy, J. (2013). Radiolabeled amino acids for oncologic imaging. *Journal of Nuclear Medicine : Official Publication, Society of Nuclear Medicine*, *54*(7), 1007–1010. https://doi.org/10.2967/JNUMED.112.113100

Huang, Y., Li, Z. Z., Huang, Y. L., Song, H. J., & Wang, Y. J. (2018). Value of free/total prostate-specific antigen (f/t PSA) ratios for prostate cancer detection in patients with total serum prostate-specific antigen between 4 and 10 ng/mL. In *Medicine (United States)* (Vol. 97, Issue 13). Lippincott Williams and Wilkins. https://doi.org/10.1097/MD.0000000000010249

Ilic, D., Evans, S. M., Allan, C. A., Jung, J. H., Murphy, D., & Frydenberg, M. (2017). Laparoscopic and robotic-assisted versus open radical prostatectomy for the treatment of localised prostate cancer. In *Cochrane Database of Systematic Reviews* (Vol. 2017, Issue 9). John Wiley and Sons Ltd. https://doi.org/10.1002/14651858.CD009625.pub2

Ilic, D., Neuberger, M. M., Djulbegovic, M., & Dahm, P. (2013). Screening for prostate cancer. *The Cochrane Database of Systematic Reviews*, *2013*(1). https://doi.org/10.1002/14651858.CD004720.PUB3

*Imaging of malignant bone involvement by morphologic, scintigraphic, and hybrid modalities - PubMed*. (n.d.). Retrieved May 29, 2022, from https://pubmed.ncbi.nlm.nih.gov/16085595/

Jambor, I., Borra, R., Kemppainen, J., Lepomäki, V., Parkkola, R., Dean, K., Alanen, K., Arponen, E., Nurmi, M., Aronen, H. J., & Minn, H. (2010). Functional imaging of localized prostate cancer aggressiveness using 11C-acetate PET/CT and 1H-MR spectroscopy. *Journal of Nuclear Medicine : Official Publication, Society of Nuclear Medicine*, *51*(11), 1676–1683. https://doi.org/10.2967/JNUMED.110.078667

Jambor, I., Borra, R., Kemppainen, J., Lepomäki, V., Parkkola, R., Dean, K., Alanen, K., Arponen, E., Nurmi, M., Aronen, H. J., & Minn, H. (2012). Improved detection of localized prostate cancer using co-registered MRI and 11C-acetate PET/CT. *European Journal of Radiology*, *81*(11), 2966–2972. https://doi.org/10.1016/J.EJRAD.2011.12.043

Jambor, I., Boström, P. J., Taimen, P., Syvänen, K., Kähkönen, E., Kallajoki, M., Perez, I. M., Kauko, T., Matomäki, J., Ettala, O., Merisaari, H., Kiviniemi, A., Dean, P. B., & Aronen, H. J. (2017). Novel biparametric MRI and targeted biopsy improves risk stratification in men with a clinical suspicion of prostate cancer (IMPROD Trial). *Journal of Magnetic Resonance Imaging : JMRI*, *46*(4), 1089–1095. https://doi.org/10.1002/JMRI.25641

Jambor, I., Kähkönen, E., Taimen, P., Merisaari, H., Saunavaara, J., Alanen, K., Obsitnik, B., Minn, H., Lehotska, V., & Aronen, H. J. (2015). Prebiopsy multiparametric 3T prostate MRI in patients with elevated PSA, normal digital rectal examination, and no previous biopsy. *Journal of Magnetic Resonance Imaging : JMRI*, *41*(5), 1394–1404. https://doi.org/10.1002/JMRI.24682

Jambor, I., Merisaari, H., Aronen, H. J., Järvinen, J., Saunavaara, J., Kauko, T., Borra, R., & Pesola, M. (2014). Optimization of b-value distribution for biexponential diffusion-weighted MR imaging of normal prostate. *Journal of Magnetic Resonance Imaging : JMRI*, *39*(5), 1213–1222. https://doi.org/10.1002/JMRI.24271

Jambor, I., Pesola, M., Merisaari, H., Taimen, P., Boström, P. J., Liimatainen, T., & Aronen, H. J. (2016). Relaxation along fictitious field, diffusion-weighted imaging, and T2 mapping of prostate cancer: Prediction of cancer aggressiveness. *Magnetic Resonance in Medicine*, *75*(5), 2130–2140. https://doi.org/10.1002/MRM.25808

Jambor, I., Pesola, M., Taimen, P., Merisaari, H., Boström, P. J., Minn, H., Liimatainen, T., & Aronen, H. J. (2016). Rotating frame relaxation imaging of prostate cancer: Repeatability, cancer detection, and Gleason score prediction. *Magnetic Resonance in Medicine*, *75*(1), 337–344. https://doi.org/10.1002/MRM.25647

Jentsch, C., Beuthien-Baumann, B., Troost, E. G. C., & Shakirin, G. (2015). Validation of functional imaging as a biomarker for radiation treatment response. *The British Journal of Radiology*, *88*(1051). https://doi.org/10.1259/BJR.20150014

Kahkonen, E., Jambor, I., Kemppainen, J., Lehtio, K., Gronroos, T. J., Kuisma, A., Luoto, P., Sipila, H. J., Tolvanen, T., Alanen, K., Silen, J., Kallajoki, M., Roivainen, A., Schafer, N., Schibli, R., Dragic, M., Johayem, A., Valencia, R., Borkowski, S., & Minn, H. (2013). In vivo imaging of prostate cancer using [68Ga]-labeled bombesin analog BAY86-7548. *Clinical Cancer Research : An Official Journal of the American Association for Cancer Research*, *19*(19), 5434–5443. https://doi.org/10.1158/1078-0432.CCR-12-3490

Kerkmeijer LGW, Groen VH, Pos FJ, Haustermans K, Monninkhof EM, Smeenk RJ, Kunze-Busch M, de Boer JCJ, van der Voort van Zijp J, van Vulpen M, Draulans C, van den Bergh L, Isebaert S, van der Heide UA. Focal boost to the intraprostatic tumor in external beam radiotherapy for patients with localized prostate cancer: results from the FLAME randomized phase III trial. *J Clin Oncol. 2021;39*(7):787–796. doi: 10.1200/JCO.20.02873. Epub 2021 Jan 20. PMID: 33471548.

Kiljunen T., Akram S., Niemelä J, Löyttyniemi E, Seppälä J., Heikkilä J., Vuolukka k., Kääriäinen OS., Heikkilä VP., Lehtiö K., Nikkinen J., Gershkevitsh E., Borkvel A., Adamson M., Zolotuhhin D., Kolk K., Pang EPP., Tuan JKL., Master Z., Chua MLK., Joensuu T., Kononen J., Myllykangas M., Riener M., Mokka M. Keyriäinen J. A deep learnining-Based Automated Anatomy for Radiation Therapy Planning A Retrospective Multicenter Study. *Diagnostics (Basel). 2020Nov 17;10(11):959.* doi:10.3390/diagnostics10110959.

Korsager, A. S., Fortunati, V., van der Lijn, F., Carl, J., Niessen, W., Østergaard, L. R., & van Walsum, T. (2015). The use of atlas registration and graph cuts for prostate segmentation in magnetic resonance images. *Medical Physics*, *42*(4), 1614–1624. https://doi.org/10.1118/1.4914379

Koschel, S., Murphy, D. G., Hofman, M. S., & Wong, L. M. (2019). The role of prostate-specific membrane antigen PET/computed tomography in primary staging of prostate cancer. *Current Opinion in Urology*, *29*(6), 569–577. https://doi.org/10.1097/MOU.0000000000000677

Koskela, K., Palmgren, J. E., Heikkilä, J., Virsunen, H., Sailas, L., Auvinen, P., Seppälä, J., & Kataja, V. (2017). Hypofractionated stereotactic body radiotherapy for localized prostate cancer - first Nordic clinical experience. *Acta Oncologica (Stockholm, Sweden)*, *56*(7), 978–983. https://doi.org/10.1080/0284186X.2017.1288923

Langmack, K. A., Perry, C., Sinstead, C., Mills, J., & Saunders, D. (2014). The utility of atlas-assisted segmentation in the male pelvis is dependent on the interobserver agreement of the structures segmented. *The British Journal of Radiology*, *87*(1043). https://doi.org/10.1259/BJR.20140299

Lecouvet, F. E., el Mouedden, J., Collette, L., Coche, E., Danse, E., Jamar, F., MacHiels, J. P., vande Berg, B., Omoumi, P., & Tombal, B. (2012). Can whole-body magnetic resonance imaging with diffusion-weighted imaging replace Tc 99m bone scanning and computed tomography for single-step detection of metastases in patients with high-risk prostate cancer? *European Urology*, *62*(1), 68–75. https://doi.org/10.1016/J.EURURO.2012.02.020

Lecouvet, F. E., Geukens, D., Stainier, A., Jamar, F., Jamart, J., D'Othée, B. J., Therasse, P., vande Berg, B., & Tombal, B. (2007). Magnetic resonance imaging of the axial skeleton for detecting bone metastases in patients with high-risk prostate cancer: diagnostic and cost-effectiveness and comparison with current detection strategies. *Journal of Clinical Oncology : Official Journal of the American Society of Clinical Oncology*, *25*(22), 3281–3287. https://doi.org/10.1200/JCO.2006.09.2940

LeCun, Y., Bengio, Y. & Hinton, G. Deep learning. *Nature* 521, 436–444 (2015). https://doi.org/10.1038/nature14539

Lee, C. H., Akin-Olugbade, O., & Kirschenbaum, A. (2011). Overview of Prostate Anatomy, Histology, and Pathology. In *Endocrinology and Metabolism Clinics of North America* (Vol. 40, Issue 3, pp. 565–575). https://doi.org/10.1016/j.ecl.2011.05.012

Logan, J. (2000). Graphical analysis of PET data applied to reversible and irreversible tracers. *Nuclear Medicine and Biology*, *27*(7), 661–670. https://doi.org/10.1016/S0969-8051(00)00137-2

Machtens, S., Serth, J., Meyer, A., Kleinhorst, C., Ommer, K.-J., Herbst, U., Kieruij, M., & Boerner, A. R. (2007). Positron emission tomography (PET) in the urooncological evaluation of the small pelvis. *World Journal of Urology*, *25*(4), 341–349. https://doi.org/10.1007/s00345-007-0194-3

Matzinger, O., Duclos, F., Bergh, A. van den, Carrie, C., Villà, S., Kitsios, P., Poortmans, P., Sundar, S., van der Steen-Banasik, E. M., Gulyban, A., Collette, L., & Bolla, M. (2009). Acute toxicity of curative radiotherapy for intermediate- and high-risk localised prostate cancer in the EORTC trial 22991. *European Journal of Cancer (Oxford, England : 1990)*, *45*(16), 2825–2834. https://doi.org/10.1016/J.EJCA.2009.07.009

Messiou, C., Collins, D. J., Giles, S., de Bono, J. S., Bianchini, D., & de Souza, N. M. (2011). Assessing response in bone metastases in prostate cancer with diffusion weighted MRI. *European Radiology*, *21*(10), 2169–2177. https://doi.org/10.1007/S00330-011-2173-8

Monninkhof, E. M., van Loon, J. W. L., van Vulpen, M., Kerkmeijer, L. G. W., Pos, F. J., Haustermans, K., van den Bergh, L., Isebaert, S., McColl, G. M., Smeenk, R. J., Noteboom, J., Walraven, I., Peeters, P. H. M., & van der Heide, U. A. (2018). Standard whole prostate gland radiotherapy with and without lesion boost in prostate cancer: Toxicity in the FLAME randomized controlled trial. *Radiotherapy and Oncology : Journal of the European Society for Therapeutic Radiology and Oncology*, *127*(1), 74–80. https://doi.org/10.1016/J.RADONC.2017.12.022

Mottet, N., Bellmunt, J., Bolla, M., Briers, E., Cumberbatch, M. G., de Santis, M., Fossati, N., Gross, T., Henry, A. M., Joniau, S., Lam, T. B., Mason, M. D., Matveev, V. B., Moldovan, P. C., van den Bergh, R. C. N., van den Broeck, T., van der Poel, H. G., van der Kwast, T. H., Rouvière, O., … Cornford, P. (2017). EAU-ESTRO-SIOG Guidelines on Prostate Cancer. Part 1: Screening, Diagnosis, and Local Treatment with Curative Intent. *European Urology*, *71*(4), 618–629. https://doi.org/10.1016/J.EURURO.2016.08.003

Nanni, C., Zanoni, L., Pultrone, C., Schiavina, R., Brunocilla, E., Lodi, F., Malizia, C., Ferrari, M., Rigatti, P., Fonti, C., Martorana, G., & Fanti, S. (2016). (18)F-FACBC (anti1-amino-3-(18)F-fluorocyclobutane-1-carboxylic acid) versus (11)C-choline PET/CT in prostate cancer relapse: results of a prospective trial. *European Journal of Nuclear Medicine and Molecular Imaging*, *43*(9), 1601–1610. https://doi.org/10.1007/S00259-016-3329-1

Njeh, C. F. Tumor delineation: The weakest link in the search for accuracy in radiotherapy. *J Med Phys* 2008, 33: 136-140. 10.4103/0971-6203.44472

Nyholm, T., Jonsson, J., Söderström, K., Bergström, P., Carlberg, A., Frykholm, G., Behrens, C. F., Geertsen, P. F., Trepiakas, R., Hanvey, S., Sadozye, A., Ansari, J., McCallum, H., Frew, J., McMenemin, R., & Zackrisson, B. (2013). Variability in prostate and seminal vesicle delineations defined on magnetic resonance images, a multi-observer, -center and -sequence study. *Radiation Oncology (London, England)*, *8*(1). https://doi.org/10.1186/1748-717X-8-126

Oyama, N., Akino, H., Kanamaru, H., Suzuki, Y., Muramoto, S., Yonekura, Y., Sadato, N., Yamamoto, K., & Okada, K. (2002). 11C-acetate PET imaging of prostate cancer. *Journal of Nuclear Medicine : Official Publication, Society of Nuclear Medicine*, *43*(2), 181–186.

Parker, C., Nilsson, S., Heinrich, D., Helle, S. I., O'Sullivan, J. M., Fosså, S. D., Chodacki, A., Wiechno, P., Logue, J., Seke, M., Widmark, A., Johannessen, D. C., Hoskin, P., Bottomley, D., James, N. D., Solberg, A., Syndikus, I., Kliment, J., Wedel, S., … Sartor, O. (2013). Alpha emitter radium-223 and survival in metastatic prostate cancer. *The New England Journal of Medicine*, *369*(3), 213–223. https://doi.org/10.1056/NEJMOA1213755

Pasquier, D., Lacornerie, T., Vermandel, M., Rousseau, J., Lartigau, E., & Betrouni, N. (2007). Automatic segmentation of pelvic structures from magnetic resonance images for prostate cancer radiotherapy. *International Journal of Radiation Oncology, Biology, Physics*, *68*(2), 592–600. https://doi.org/10.1016/J.IJROBP.2007.02.005

Perera M, Papa N, Christidis D, Wetherell D, Hofman MS, Murphy DG, Bolton D, Lawrentschuk N. Sensitivity, Specificity, and Predictors of Positive $^{68}$Ga-Prostate-specific Membrane Antigen Positron Emission Tomography in Advanced Prostate Cancer: A Systematic Review and Meta-analysis. *Eur Urol. 2016 Dec;70*(6):926-937. doi: 10.1016/j.eururo.2016.06.021. Epub 2016 Jun 28. PMID: 27363387.

Pike, V. W., Eakins, M. N., Allan, R. M., & Selwyn, A. P. (1982). Preparation of [1-11C]acetate--an agent for the study of myocardial metabolism by positron emission tomography. *The International*

*Journal of Applied Radiation and Isotopes*, *33*(7), 505–512. https://doi.org/10.1016/0020-708X(82)90003-5

Qayyum, A. (2009). Diffusion-weighted imaging in the abdomen and pelvis: concepts and applications. *Radiographics : A Review Publication of the Radiological Society of North America, Inc*, *29*(6), 1797–1810. https://doi.org/10.1148/RG.296095521

Rasch C, Steenbakkers R, van Herk M: Target Definition in Prostate, Head, and Neck. *Semin Radiat Oncol* 2005, 15: 136-145. 10.1016/j.semradonc.2005.01.005

Roodman GD. Mechanisms for Bone Metastasis. *Discov. Med. 2004 Jun;4*(22):144-8. PMID:20704976. DOI: 10.1056/NEJMra030831

Rosenkrantz, A. B., Kim, S., Lim, R. P., Hindman, N., Deng, F. M., Babb, J. S., & Taneja, S. S. (2013). Prostate cancer localization using multiparametric MR imaging: Comparison of Prostate Imaging Reporting and Data System (PI-RADS) and Likert scales. *Radiology*, *269*(2), 482–492. https://doi.org/10.1148/RADIOL.13122233/-/DC1

Rutter, C. M. (2000). Bootstrap estimation of diagnostic accuracy with patient-clustered data. *Academic Radiology*, *7*(6), 413–419. https://doi.org/10.1016/S1076-6332(00)80381-5

Salembier, C., Villeirs, G., de Bari, B., Hoskin, P., Pieters, B. R., van Vulpen, M., Khoo, V., Henry, A., Bossi, A., de Meerleer, G., & Fonteyne, V. (2018). ESTRO ACROP consensus guideline on CT- and MRI-based target volume delineation for primary radiation therapy of localized prostate cancer. *Radiotherapy and Oncology : Journal of the European Society for Therapeutic Radiology and Oncology*, *127*(1), 49–61. https://doi.org/10.1016/J.RADONC.2018.01.014

Sharp, G.; Fritscher, K.D.; Pekar, V.; Peroni, M.; Shusharina, N.; Veeraraghavan, H.; Yang, J. Vision 20/20:Perspectives on automated image segmentation for radiotherapy. *Med. Phys. 2014, 41, 050902*. DOI: 10.1118/1.4871620

Schimmöller, L., Quentin, M., Arsov, C., Lanzman, R. S., Hiester, A., Rabenalt, R., Antoch, G., Albers, P., & Blondin, D. (2013). Inter-reader agreement of the ESUR score for prostate MRI using in-bore MRI-guided biopsies as the reference standard. *European Radiology*, *23*(11), 3185–3190. https://doi.org/10.1007/S00330-013-2922-Y

Schirrmeister, H., Glatting, G., Hetzel, J., Nüssle, K., Arslandemir, C., Buck, A. K., Dziuk, K., Gabelmann, A., Reske, S. N., & Hetzel, M. (2001). Prospective evaluation of the clinical value of planar bone scans, SPECT, and (18)F-labeled NaF PET in newly diagnosed lung cancer. *Journal of Nuclear Medicine : Official Publication, Society of Nuclear Medicine*, *42*(12), 1800–1804. https://pubmed.ncbi.nlm.nih.gov/11752076/

Schmidt, G. P., Schoenberg, S. O., Schmid, R., Stahl, R., Tiling, R., Becker, C. R., Reiser, M. F., & Baur-Melnyk, A. (2007). Screening for bone metastases: whole-body MRI using a 32-channel system versus dual-modality PET-CT. *European Radiology*, *17*(4), 939–949. https://doi.org/10.1007/S00330-006-0361-8

Schmidt, M. A., & Payne, G. S. (2015). Radiotherapy planning using MRI. *Physics in Medicine and Biology*, *60*(22), R323–R361. https://doi.org/10.1088/0031-9155/60/22/R323

Schulz, J., Skrøvseth, S. O., Tømmerås, V. K., Marienhagen, K., & Godtliebsen, F. (2014). *Open Access A semiautomatic tool for prostate segmentation in radiotherapy treatment planning*.

Schumacher, M. C., Radecka, E., Hellström, M., Jacobsson, H., & Sundin, A. (2015). [11C]Acetate positron emission tomography-computed tomography imaging of prostate cancer lymph-node metastases correlated with histopathological findings after extended lymphadenectomy. *Scandinavian Journal of Urology*, *49*(1), 35–42. https://doi.org/10.3109/21681805.2014.932840

Schuster, D. M., Nanni, C., & Fanti, S. (2016). PET Tracers Beyond FDG in Prostate Cancer. *Seminars in Nuclear Medicine*, *46*(6), 507–521. https://doi.org/10.1053/J.SEMNUCLMED.2016.07.005

Schuster, D. M., Nieh, P. T., Jani, A. B., Amzat, R., Bowman, F. D., Halkar, R. K., Master, V. A., Nye, J. A., Odewole, O. A., Osunkoya, A. O., Savir-Baruch, B., Alaei-Taleghani, P., & Goodman, M. M. (2014). Anti-3-[18F]FACBC positron emission tomography-computerized tomography and 111In-capromab pendetide single photon emission computerized tomography-computerized

tomography for recurrent prostate carcinoma: Results of a prospective clinical trial. *Journal of Urology*, *191*(5), 1446–1453. https://doi.org/10.1016/j.juro.2013.10.065

Schuster, D. M., Taleghani, P. A., Nieh, P. T., Master, V. A., Amzat, R., Savir-Baruch, B., Halkar, R. K., Fox, T., Osunkoya, A. O., Moreno, C. S., Nye, J. A., Yu, W., Fei, B., Wang, Z., Chen, Z., & Goodman, M. M. (2013). Characterization of primary prostate carcinoma by anti-1-amino-2-[(18)F] -fluorocyclobutane-1-carboxylic acid (anti-3-[(18)F] FACBC) uptake. *American Journal of Nuclear Medicine and Molecular Imaging*, *3*(1), 85–96. https://pubmed.ncbi.nlm.nih.gov/23342303/

Seppälä, J., Seppänen, M., Arponen, E., Lindholm, P., & Minn, H. (2009). Carbon-11 acetate PET/CT based dose escalated IMRT in prostate cancer. *Radiotherapy and Oncology : Journal of the European Society for Therapeutic Radiology and Oncology*, *93*(2), 234–240. https://doi.org/10.1016/J.RADONC.2009.08.010

Shen, G., Deng, H., Hu, S., & Jia, Z. (2014). Comparison of choline-PET/CT, MRI, SPECT, and bone scintigraphy in the diagnosis of bone metastases in patients with prostate cancer: a meta-analysis. *Skeletal Radiology*, *43*(11), 1503–1513. https://doi.org/10.1007/S00256-014-1903-9

Sörensen, J., Owenius, R., Lax, M., & Johansson, S. (2013). Regional distribution and kinetics of [18F]fluciclovine (anti-[18F]FACBC), a tracer of amino acid transport, in subjects with primary prostate cancer. *European Journal of Nuclear Medicine and Molecular Imaging*, *40*(3), 394–402. https://doi.org/10.1007/S00259-012-2291-9

Stamey, T. A., Yang, N., Hay, A. R., McNeal, J. E., Freiha, F. S., & Redwine, E. (1987). Prostate-specific antigen as a serum marker for adenocarcinoma of the prostate. *The New England Journal of Medicine*, *317*(15), 909–916. https://doi.org/10.1056/NEJM198710083171501

Sung, H., Ferlay, J., Siegel, R. L., Laversanne, M., Soerjomataram, I., Jemal, A., & Bray, F. (2021). Global Cancer Statistics 2020: GLOBOCAN Estimates of Incidence and Mortality Worldwide for 36 Cancers in 185 Countries. *CA: A Cancer Journal for Clinicians*, *71*(3), 209–249. https://doi.org/10.3322/CAAC.21660

Sweat, S. D., Pacelli, A., Murphy, G. P., & Bostwick, D. G. (1998). Prostate-specific membrane antigen expression is greatest in prostate adenocarcinoma and lymph node metastases. *Urology*, *52*(4), 637–640. https://doi.org/10.1016/S0090-4295(98)00278-7

Thomsen, F. B., Brasso, K., Klotz, L. H., Røder, M. A., Berg, K. D., & Iversen, P. (2014). Active surveillance for clinically localized prostate cancer--a systematic review. *Journal of Surgical Oncology*, *109*(8), 830–835. https://doi.org/10.1002/JSO.23584

Toivonen, J., Merisaari, H., Pesola, M., Taimen, P., Boström, P. J., Pahikkala, T., Aronen, H. J., & Jambor, I. (2015). Mathematical models for diffusion-weighted imaging of prostate cancer using b values up to 2000 s/mm(2) : correlation with Gleason score and repeatability of region of interest analysis. *Magnetic Resonance in Medicine*, *74*(4), 1116–1124. https://doi.org/10.1002/MRM.25482

Trajman, A., & Luiz, R. R. (2008). McNemar chi2 test revisited: comparing sensitivity and specificity of diagnostic examinations. *Scandinavian Journal of Clinical and Laboratory Investigation*, *68*(1), 77–80. https://doi.org/10.1080/00365510701666031

Treglia, G., Annunziata, S., Pizzuto, D. A., Giovanella, L., Prior, J. O., & Ceriani, L. (2019). Detection Rate of 18 F-Labeled PSMA PET/CT in Biochemical Recurrent Prostate Cancer: A Systematic Review and a Meta-Analysis. *Cancers*, *11*(5). https://doi.org/10.3390/CANCERS11050710

Turkbey, B., Mena, E., Shih, J., Pinto, P. A., Merino, M. J., Lindenberg, M. L., Bernardo, M., McKinney, Y. L., Adler, S., Owenius, R., Choyke, P. L., & Kurdziel, K. A. (2014). Localized prostate cancer detection with 18F FACBC PET/CT: comparison with MR imaging and histopathologic analysis. *Radiology*, *270*(3), 849–856. https://doi.org/10.1148/RADIOL.13130240

Ulmert, D., Solnes, L., & Thorek, D. L. (2015). Contemporary approaches for imaging skeletal metastasis. *Bone Research*, *3*(1). https://doi.org/10.1038/BONERES.2015.24

Uprimny, C., Kroiss, A. S., Decristoforo, C., Fritz, J., von Guggenberg, E., Kendler, D., Scarpa, L., di Santo, G., Roig, L. G., Maffey-Steffan, J., Horninger, W., & Virgolini, I. J. (2017). 68 Ga-PSMA-11 PET/CT in primary staging of prostate cancer: PSA and Gleason score predict the intensity of tracer accumulation in the primary tumour. *European Journal of Nuclear Medicine and Molecular Imaging*, *44*(6), 941–949. https://doi.org/10.1007/S00259-017-3631-6

Vanel, D., Bittoun, J., & Tardivon, A. (1998). MRI of bone metastases. *European Radiology*, *8*(8), 1345–1351. https://doi.org/10.1007/S003300050549

Viani, G. A., Stefano, E. J., & Afonso, S. L. (2009). Higher-than-conventional radiation doses in localized prostate cancer treatment: a meta-analysis of randomized, controlled trials. *International Journal of Radiation Oncology, Biology, Physics*, *74*(5), 1405–1418. https://doi.org/10.1016/J.IJROBP.2008.10.091

von Eyben, F. E., & Kairemo, K. (2014). Meta-analysis of (11)C-choline and (18)F-choline PET/CT for management of patients with prostate cancer. *Nuclear Medicine Communications*, *35*(3), 221–230. https://doi.org/10.1097/MNM.0000000000000040

Vora, S. A., Wong, W. W., Schild, S. E., Ezzell, G. A., & Halyard, M. Y. (2007). Analysis of biochemical control and prognostic factors in patients treated with either low-dose three-dimensional conformal radiation therapy or high-dose intensity-modulated radiotherapy for localized prostate cancer. *International Journal of Radiation Oncology, Biology, Physics*, *68*(4), 1053–1058. https://doi.org/10.1016/J.IJROBP.2007.01.043

Wang, Z., Ni, Y., Chen, J., Sun, G., Zhang, X., Zhao, J., Zhu, X., Zhang, H., Zhu, S., Dai, J., Shen, P., & Zeng, H. (2020). The efficacy and safety of radical prostatectomy and radiotherapy in high-risk prostate cancer: a systematic review and meta-analysis. *World Journal of Surgical Oncology*, *18*(1). https://doi.org/10.1186/S12957-020-01824-9

Weinreb JC, Barentsz JO, Choyke PL, Cornud F, Haider MA, Macura KJ, et al. PI-RADS Prostate Imaging - Reporting and Data System: 2015, Version 2. *Eur Urol. 2016;69*(1):16–40. https://doi.org/10.1016/j.eururo.2015.08.052

Wong, J., Fong, A., McVicar, N., Smith, S., Giambattista, J., Wells, D., Kolbeck, C., Giambattista, J., Gondara, L., & Alexander, A. (2020). Comparing deep learning-based auto-segmentation of organs at risk and clinical target volumes to expert inter-observer variability in radiotherapy planning. *Radiotherapy and Oncology : Journal of the European Society for Therapeutic Radiology and Oncology*, *144*, 152–158. https://doi.org/10.1016/J.RADONC.2019.10.019

Yadav, M. P., Ballal, S., Sahoo, R. K., Dwivedi, S. N., & Bal, C. (2019). Radioligand Therapy With 177 Lu-PSMA for Metastatic Castration-Resistant Prostate Cancer: A Systematic Review and Meta-Analysis. *AJR. American Journal of Roentgenology*, *213*(2), 275–285. https://doi.org/10.2214/AJR.18.20845

Yu JB., Soulos PR, Herrin J., Crames LD., Potosky AL., Roberts KB., Gross SP. Proton versus intensity-modulated radiotherapy for prostate cancer: patterns of care and early toxicity. *J Natl Cancer Inst. 2013 Jan 2;105*(1):25-32. doi: 10.1093/jnci/djs463. Epub 2012 Dec 14. PMID: 23243199; PMCID: PMC3536640

Zelefsky, M. J., Levin, E. J., Hunt, M., Yamada, Y., Shippy, A. M., Jackson, A., & Amols, H. I. (2008). Incidence of late rectal and urinary toxicities after three-dimensional conformal radiotherapy and intensity-modulated radiotherapy for localized prostate cancer. *International Journal of Radiation Oncology, Biology, Physics*, *70*(4), 1124–1129. https://doi.org/10.1016/J.IJROBP.2007.11.044

Zijdenbos, A. P., Dawant, B. M., Margolin, R. A., & Palmer, A. C. (1994). Morphometric analysis of white matter lesions in MR images: method and validation. *IEEE Transactions on Medical Imaging*, *13*(4), 716–724. https://doi.org/10.1109/42.363096

# Original Publications

**Jambor I, Kuisma A, Kähkönen E, Kemppainen J, Merisaari H, Eskola O, Teuho J, Perez I M, Pesola M, Aronen H J, Boström P J, Taimen P & Minn H (2018)**
**Prospective evaluation of $^{18}$F-FACBC PET/CT and PET/MRI versus multiparametric MRI in intermediate- to high-risk prostate cancer patients (FLUCIPRO trial).**
Eur J Nucl Med Mol Imaging

I

**Jambor I, Kuisma A, Ramadan S, Huovinen R, Sandell M, Kanjander S, Kemppainen J, Kauppila E, Auren J, Merisaari H, Saunavaara J, Noponen T, Minn H, J. Aronen H J & Seppänen M (2016)**
**Prospective evaluation of planar bone scintigraphy SPECT, SPECT/CT, $^{18}$F-NaF PET/ CT and whole body 1.5T MRI, including, DWI for the detection of bone metastases in high risk breast and prostate cancer patients: SKELETA clinical trial.**
Acta Oncologica

**II**

**Kuisma A, Ranta I, Keyriläinen J, Suilamo S, Wright P, Pesola M, Warner L, Löyttyniemi E & Minn H (2020)**
**Validation of automated magnetic resonance image segmentation for radiation therapy planning in prostate cancer.**
Physics and Imaging in Radiation Oncology

**III**

**Kuisma A, Wright P, Suilamo S, Seppälä J, Koivisto M, Lindholm P & Minn H (2022)**
**Long-term outcome of biologically guided dose-escalated radiotherapy of localized prostate cancer.**
ActaOncologica

IV

TURUN
YLIOPISTO
UNIVERSITY
OF TURKU

Painosalama, Turku, Finland 2023

ISBN 978-951-29-9137-2 (PRINT)
ISBN 978-951-29-9138-9 (PDF)
ISSN 0355-9483 (Print)
ISSN 2343-3213 (Online)